

South Dakota State University

Open PRAIRIE: Open Public Research Access Institutional Repository and Information Exchange

Electronic Theses and Dissertations

2022

The Significance of a New 11,000-Year Volcanic Record from the South Pole and Inferences from Comparisons with Other Volcanic Records

Derek Lee Brandis

South Dakota State University, dbrandis@jacks.sdstate.edu

Follow this and additional works at: <https://openprairie.sdstate.edu/etd2>



Part of the [Environmental Chemistry Commons](#), [Oceanography and Atmospheric Sciences and Meteorology Commons](#), and the [Volcanology Commons](#)

Recommended Citation

Brandis, Derek Lee, "The Significance of a New 11,000-Year Volcanic Record from the South Pole and Inferences from Comparisons with Other Volcanic Records" (2022). *Electronic Theses and Dissertations*. 446.

<https://openprairie.sdstate.edu/etd2/446>

This Dissertation - Open Access is brought to you for free and open access by Open PRAIRIE: Open Public Research Access Institutional Repository and Information Exchange. It has been accepted for inclusion in Electronic Theses and Dissertations by an authorized administrator of Open PRAIRIE: Open Public Research Access Institutional Repository and Information Exchange. For more information, please contact michael.biondo@sdstate.edu.

THE SIGNIFICANCE OF A NEW 11,000-YEAR VOLCANIC RECORD FROM THE
SOUTH POLE AND INFERENCES FROM COMPARISONS WITH OTHER
VOLCANIC RECORDS

BY

DEREK LEE BRANDIS

A dissertation submitted in partial fulfillment of the requirements for the

Doctor of Philosophy

Major in Chemistry

South Dakota State University

2022

DISSERTATION ACCEPTANCE PAGE

Derek Lee Brandis

This dissertation is approved as a creditable and independent investigation by a candidate for the Doctor of Philosophy degree and is acceptable for meeting the dissertation requirements for this degree. Acceptance of this does not imply that the conclusions reached by the candidate are necessarily the conclusions of the major department.

Jihong Cole-Dai
Advisor

Date

Douglas Raynie
Department Head

Date

Nicole Lounsbury, PhD
Director, Graduate School

Date

Dedicated to my parents
Marvin and Arlene Brandis
who are forever in my heart.

ACKNOWLEDGEMENTS

As I reach the culmination of my doctoral degree, I have had the support of so many people to reach this point. My path to this degree has not been straightforward and has had many challenges. Yet the support from family, friends, colleagues, and mentors along the way helped and encouraged me to finish this degree.

This entire project would not have been possible without the support and guidance of my advisor, Dr. Jihong Cole-Dai. I think about the beginning of my graduate studies to where I am now, and I have learned so much being a part of the ICECL lab group. From learning ice core laboratory skills to preparing drafts and presentations, your patience and willingness to answer questions has allowed me to become a true scientist who is excited about my career path going forward. Thank you so much for allowing me to be a part of your lab group and helping me every step of the way.

Many people within the Department of Chemistry & Biochemistry deserve thanks as well. To Stephanie Jensen and Jaque Mann, thank you for helping me with any questions I had and always lending an ear when I needed advice. To my committee members, Dr. Matt Miller, Dr. Brian Logue, and Dr. Ann Michelle-Daniels, thank you for your guidance. To the members of the ICECL lab group, the Department as a whole, and the SDSU American Indian Student Center, thank you for your support.

To all my friends near and far, thank you so much for being there for me when needed and helping me to stay positive throughout this process. The many good times we've had and the laughs we've shared will never be forgotten.

Last, thank you to my family, especially my parents. Mom and dad, without your unconditional support and encouragement I would not have been able to finish this degree. I wish I was able to celebrate my doctoral graduation and the culmination of this entire process with you in person, but I know you are with me each and every day. Please continue to watch out for me until we see each other again.

TABLE OF CONTENTS

LIST OF FIGURES	viii
LIST OF TABLES	x
ABSTRACT	xi
1. INTRODUCTION	1
1.1 Volcanism.....	1
1.2 Ice Cores.....	2
1.3 Sulfate in Antarctic Snow	4
1.4 Project Goal & Objectives.....	5
2. METHODS	7
2.1 Ice Core Collection.....	7
2.2 Labware Cleaning Procedures.....	8
2.3 Sample Melting and Collection.....	9
2.4 Sample Depth Tracking.....	11
2.5 Major Ion Analysis and Ion Chromatography.....	12
2.6 Ice Core Dating	14
2.6.1 SP19 Dating Accuracy	16
2.6.2 SP19 Dating Uncertainty	18
2.7 Sources of Sulfate in Antarctic Snow	21
2.8 Sulfate Flux	23
2.9 Ice Sheet Thinning Consideration	25
3. RESULTS	27
3.1 SPC14 Sulfate Flux Dataset	27

3.1.1	SPC14 Volcanic Detection Threshold	28
3.1.2	SPC14 Sulfate Background.....	33
3.2	Volcanic Flux of Volcanic Events	34
3.3	Frequency of Events.....	36
3.4	Largest Events by Volcanic Flux in SPVR2022	37
3.5	Event Comparison Using Volcanic Flux.....	38
3.6	SPC14 Relative Flux	40
3.7	SPVR2022 Total Volcanic Flux and Events	41
4.	DISCUSSION.....	44
4.1	Event Frequency During the Last 2000 years	44
4.1.1	Detection Threshold Methodologies for Plateau Remote & Dome C	46
4.1.2	Detection Threshold Methodologies for WHV2020 & SPVR2022	47
4.2	Holocene Event Frequency Comparison of SPV2022 to WHV2020	48
4.2.1	Eruption Frequency Statistical Comparison	49
4.3	Ten Largest Volcanic Events in SPVR2022 & WHV2020.....	51
4.3.1	Differences in the Largest Events in SPVR2022 & WHV2020	53
4.4	Volcanic Events and the Santorini (Thera) Eruption in 17th Century BCE	54
5.	CONCLUSIONS.....	58
	APPENDIX A – SPVR2022.....	60
	REFERENCES	70

LIST OF FIGURES

Figure 1. Ice core section and bandsaw cut locations (top), and chemical analysis stick with dimensions (bottom).	7
Figure 2. Melter schematic showing a top view (left) and side view (right).	10
Figure 3. Schematic of continuous ice core melter system.....	11
Figure 4. Ion chromatography system components and flow path.	12
Figure 5. Cation chromatogram with retention times of sodium (Na^+), potassium (K^+), magnesium (Mg^{2+}), and calcium (Ca^{2+}).....	13
Figure 6. Anion chromatogram with retention times of chloride (Cl^-), nitrate (NO_3^-), and sulfate (SO_4^{2-}).....	13
Figure 7. Cyclic variation of sodium from 326.0 m to 327.0 m.	14
Figure 8. Volcanic tie point in SP19 (top, black) and WD2014 (bottom, blue).	17
Figure 9. ALC precision example from SP14 using sodium from 232.0m to 233.0m. Blue circle indicates a potentially uncertain year.	19
Figure 10. SP19 timescale uncertainty determination during the Holocene. Light blue area represents WD2014 uncertainty, blue line represents SP19 uncertainty, and black line represents total uncertainty in SP19. Red box indicates portions of largest uncertainty between volcanic tie points in SP19.	21
Figure 11. Cyclic variation of sulfate in SP14 from 326.0 m to 327.0 m.....	22
Figure 12. Annual non-sea-salt sulfate flux in the Holocene for the SP14.....	27
Figure 13. Magnified view of SP14 nss-sulfate flux data with mean as the non-volcanic background and mean plus two times the standard deviation as the threshold.	29
Figure 14. SP14 volcanic record with 41-pt RM.	30

Figure 15. SP14 RM and detection threshold for 8000-9000 BP.	32
Figure 16. SP14 background nss-sulfate after removal of volcanic events.	33
Figure 17. Background nss-sulfate w/RRM from 8000 to 9000 years BP.	34
Figure 18. Number of events by millennium in SPC14.	36
Figure 19. Ice core locations in Antarctica where Tambora volcanic flux has been measured.	39
Figure 20. SPVR2022 total millennial volcanic flux and number of events comparison.	42
Figure 21. Number of events during the last 2000 years for different Antarctica ice core drilling sites.	44
Figure 22. SPVR2022 & WHV2020 millennia event frequency comparison.	48

LIST OF TABLES

Table 1. Volcanic flux event examples.	35
Table 2. Ten largest events by volcanic flux in SPVR2022.....	37
Table 3. Antarctica volcanic flux for Tambora.	39
Table 4. Comparison of volcanic flux and relative flux for the 1458/1459 event in two Antarctic volcanic records.	41
Table 5. SPVR2022 total millennial volcanic flux and number of events for every 1000 years BP.	43
Table 6. Event frequency in SPVR2022 & WHV2020 for every 1000 years in the Holocene.	49
Table 7. t-test statistical values.	50
Table 8. Ten largest events by relative flux in SPVR2022.	51
Table 9. Ten largest events by relative flux in WHV2020.....	52
Table 10. Potential Thera comparison in SPVR2022 & WHV2020.....	56

ABSTRACT

THE SIGNIFICANCE OF A NEW 11,000-YEAR VOLCANIC RECORD FROM THE
SOUTH POLE AND INFERENCES FROM COMPARISONS WITH OTHER
VOLCANIC RECORDS

DEREK LEE BRANDIS

2022

Snow accumulation at the polar regions of the planet preserves chemical substances from the atmosphere creating natural archives. Records of the atmospheric environment including atmospheric chemical composition and the climate can be reconstructed from ice cores from the polar ice sheets. Sulfur emitted by explosive volcanic eruptions is preserved as sulfate in polar snow and can be used to reconstruct the record of volcanic eruptions. Since large volcanic eruptions impact the environment and climate, records of volcanic eruptions from ice cores can help us to study and understand climate change and model the future climate environment.

A 1750-m ice core was drilled at the South Pole (SPC14), and major ion analysis was performed via capillary ion chromatography on ice samples. The sulfate data was then used to create a new 11,000-year record of volcanic eruptions from this ice core: the 2022 SPICEcore Volcanic Record, SPVR2022. While other Antarctic ice core records exist, this is the first detailed and quantitative record from a South Pole ice core covering the entire Holocene period (last 11 ka years). The objectives of this dissertation project were: 1) the detection and extraction of signals representing volcanic eruptions from the sulfate data to create SPVR2022, and 2) investigation of the similarities and differences between

SPVR2022 and other Antarctic ice core volcanic records, including event frequency, statistical analysis, and relative flux of volcanic sulfate.

SPVR2022 shows the number of events within the last 2000 years are similar to that in the high-resolution volcanic record (WHV2020) from the West Antarctic Ice Sheet (WAIS) Divide ice core. No apparent trend is seen in the frequency of events during the Holocene period in SPVR2022, and no statistical difference in the frequency of events in each millennium is found between SPVR2022 and WHV2020. The ten largest events in SPVR2022 show similarities and differences to the ten largest events in WHV2020. Differences may be attributed to different glaciological environments such as snow accumulation rate and elevation, or to atmospheric transport processes such as the polar vortex. Understanding why these differences exist will be beneficial to the understanding the volcano-climate connection.

1. INTRODUCTION

1.1 Volcanism

Volcanic eruptions can affect not only the areas around the volcanoes, but also the entire planet depending on the location of the volcano and the magnitude of the eruption. Eruptions release hot magma, ash, and gases which can threaten life in the immediate vicinity of the volcano. If the eruption is large enough, ash and gases such as carbon dioxide and sulfur dioxide can be injected into the stratosphere. Unlike the volcanic ash that is deposited back to the ground via gravity shortly after an eruption, gases remain in the atmosphere for extended times. Atmospheric winds can carry the gases much farther from the site of the volcano and to every part of the atmosphere. While in the atmosphere, sulfur dioxide is converted to sulfuric acid and subsequently to sulfate aerosols. The sulfate aerosols can result in direct climate forcing by reflecting solar radiation back into space (Kiehl and Brieglab, 1993).

The potential of large volcanic eruption's effect on global climate was studied in the early 1960s using annual and winter means of temperature in the form of 5-year averages (Mitchell, 1961). The residence time of the ash and gases from volcanic eruptions was thought to be similar to that of the residence time of bomb debris which was believed to be depleted from the atmosphere within 5 years (Stebbins, 1960). The results the Stebbins study showed a consistent tendency for large volcanic eruptions to lower the temperature of the hemisphere of eruption for a period of time. However, very little material that is injected into the atmosphere in one hemisphere will cross the equator into the other hemisphere (Stebbins, 1960). Yet, major volcanic eruptions in the tropics can affect both the northern and southern hemispheres. The large amount of sulfate aerosols

in the stratosphere from explosive volcanic eruptions cools the planet for a period of time. The sulfate aerosol particles (with residence times of up to 3 years) are similar in size to that of visible light (0.5 μm effective radius), thus strongly interacting with light by scattering and increasing the planet's albedo causing the planet to cool (Robock, 2000, Robock, 2003).

1.2 Ice Cores

While direct observations of eruptions yield real-time datasets (measurements of sulfate aerosol mass, radiative forcing, temperature response, etc.) about the relationship with climate, these types of datasets are limited to more recent times. However, data would be beneficial for very large eruptions that occurred in the past before written record and direct observation. The evidence of volcanic eruptions may be preserved in and retrieved from some environmental media. Since the fallout from a volcanic eruption is eventually deposited back to the planet's surface, media that could preserve this fallout would be useful. Charcoal and lava flow sampling has been used to determine when large volcanic events took place; yet, the limited amount of datable material and the complex relationship with volcanic impact presents challenges to using this method (Rodriguez-Gonzalez *et al.*, 2009). An ideal media would preserve the fallout from volcanic eruptions which can be measured and would allow for the creation of a highly accurate and precise chronological record.

Chemical compounds present in the atmosphere can become trapped in precipitation and are eventually deposited back to the earth's surface. At the polar regions of the planet this occurs through snow which accumulates continuously creating a natural

archive of the atmospheric composition. As the snow layers build over time, they eventually become ice due to the pressure from the layers above.

One of the first studies to examine a polar natural archive was via a 15 m snow pit study performed in Greenland in the early 1930s (Sorge, 1932). Nearly 20 years later, three separate research teams traveled to Antarctica, Greenland, and Alaska with mechanical drills to go deeper into ice sheets to collect samples of approximately one hundred meters – the first ice cores (Langway, 2008). Ice cores from these regions provide a way to extract information from these archives to study past atmospheric conditions. This information can be used to create chronological records from ice cores.

Large volcanic eruptions release substantial amounts of sulfur dioxide, which is converted to sulfate aerosols in the atmosphere, and can be seen in ice cores as signals of elevated sulfate concentrations. While sulfate measured in ice cores can determine the forcing of volcanic events, other natural archives such as tree rings can also be used to see the impact of large volcanic eruptions. However, in the case of tree rings, they can only show a period of cooling caused by the eruption. Ice cores have the benefit of not only showing the sulfate ejected in a large eruption as the cause of cooling (climate forcing), but also showing the effect, i.e. cooling, resulting from the cause/forcing (impact) (Kennedy, 2020).

The capability of ice cores to infer atmospheric composition varies depending on some characteristics such as location, property parameters measured, and dating accuracy. For example, while snow accumulation at the polar regions creates stratigraphic layers within the ice sheet, snow accumulation rate differs from location to location. The accumulation rate at the West Antarctica Ice Sheet Divide (WAIS Divide) is approximately

21 centimeters water equivalent per year (cm w.e. y^{-1}) while the South Pole receives closer to 8 cm w.e. y^{-1} on average (Banta *et al.*, 2008, Mosley-Thompson and Thompson, 1982). Higher accumulation sites allow for much better sample resolution, whereas lower accumulation sites allow longer temporal records to be created. This occurs because higher accumulation sites allow more samples to be analyzed within a year than at a low accumulation site, creating better sub-annual resolution. In addition, at greater depths the layers become compressed and high accumulation sites will have thicker layers at these depths allowing more samples to be collected across the layer.

Another factor to consider is the chemical or physical processes that affect how information about the atmosphere is encoded in snow and how chemical substances bearing the information become embedded in polar snow. Ice core locations in the Northern Hemisphere (specifically Greenland) can capture anthropogenic processes better to due to its proximity to populous continents and landmasses in the Northern Hemisphere. Natural processes, such as sea-salt, tend to be more visible in ice cores from Antarctica as there is less landmass and anthropogenic processes in the Southern Hemisphere within close proximity to Antarctica.

Overall, ice cores are very good for assessing both volcanic forcing and climate impact, but other factors such as snowfall accumulation rate and the chemical and physical properties of interest can play an important role in where to drill for ice cores (site selection).

1.3 Sulfate in Antarctic Snow

Atmospheric sulfate comes from both natural and anthropogenic sources. Natural sources consist of emissions of dimethyl sulfide (DMS) by marine biogenic organisms

(phytoplankton) and sulfur dioxide emissions from volcanic eruptions, while anthropogenic sources are attributed to combustion byproducts (Sofen *et al.*, 2011). In addition, continental dust and sea-salt can also contribute to the total sulfate budget (Legrand and Mayewski, 1997). While all these contribute to the overall sulfate budget, the relative contributions by individual sources depend on the location. For example, the fact that Antarctica is not influenced by anthropogenic sources makes it a more desirable location for the study of natural sulfate sources.

While Antarctica offers a pristine environment for the study of sulfate from volcanic eruptions, the concentrations in snow and ice samples are not high: total sulfate concentrations in Antarctic snow have been found to range from 10 to 200 nanograms per gram (Legrand, 1995). Large spikes in sulfate concentrations can indicate a volcanic eruption took place due to the large amounts of sulfur dioxide released into the atmosphere by explosive eruptions. However, small volcanic events may increase the sulfate level in snow slightly above the natural background level; these events may be better quantified than the same events in other ice cores due to the levels of natural sulfate concentrations found on the Antarctic ice sheet. In any case, if the natural background sulfate level could be determined, the amount of sulfate from a volcanic eruption could be determined as well.

1.4 Project Goal & Objectives

The goal of this project is to improve the understanding of volcanic eruptions and their effects on climate. Volcanic records from ice cores are valuable to studying the climate since ice cores are natural archives preserving chemical species in the snow strata which can then be used to study the volcano-climate relationship (Ferris *et al.*, 2011). The volcanic records from ice cores can be analyzed to provide data such as the date an eruption

occurred and the magnitude of the eruption, data which can then be used to investigate past climate perturbations (Cole-Dai, 2010, Gao *et al.*, 2006).

A volcanic record from the South Pole is important since volcanic signals can vary appreciably among ice cores due to differences between ice cores from various locations in atmospheric transport of sulfate aerosols to the ice core location, sulfate aerosol preservation within snow strata, and signal detection and quantitation (Cole-Dai *et al.*, 2021). Other ice core studies exist that have advanced this understanding, but no detailed South Pole volcanic record covering the Holocene currently exists. The primary objective of this project is to establish a detailed and quantitative record of volcanic events in the Holocene period from a recently drilled South Pole ice core. A secondary objective is to compare, contrast, and investigate how the new record compares to existing records. Investigating why differences exist between the new volcanic record and other ice core volcanic records will help advance the discussion of glaciological conditions which may influence sulfate deposit and also help advance the discussion of the volcano-climate connection.

2. METHODS

2.1 Ice Core Collection

The intermediate South Pole Ice Core (SPICEcore) is a 1751-meter ice core that was recovered from a location approximately 2.7 km west of the Amundsen-Scott South Pole Station (90°S) with the exact coordinates of the drill site being 89.99° S, 98.16° W. The SPICEcore (SPC14) was drilled over two austral summer seasons: 2014/2015 (surface to 755 meters) and 2015/2016 (755 to 1751 meters) (Winski *et al.*, 2019a). The 98 mm diameter core was drilled in two-meter sections using the intermediate-depth drill (IDD) developed at the University of Wisconsin-Madison by the Ice Drilling Design and Operations (IDDO) group (Johnson *et al.*, 2017). The two-meter section was then cut into one-meter sections (Figure 1), and each one-meter section was processed in the field,

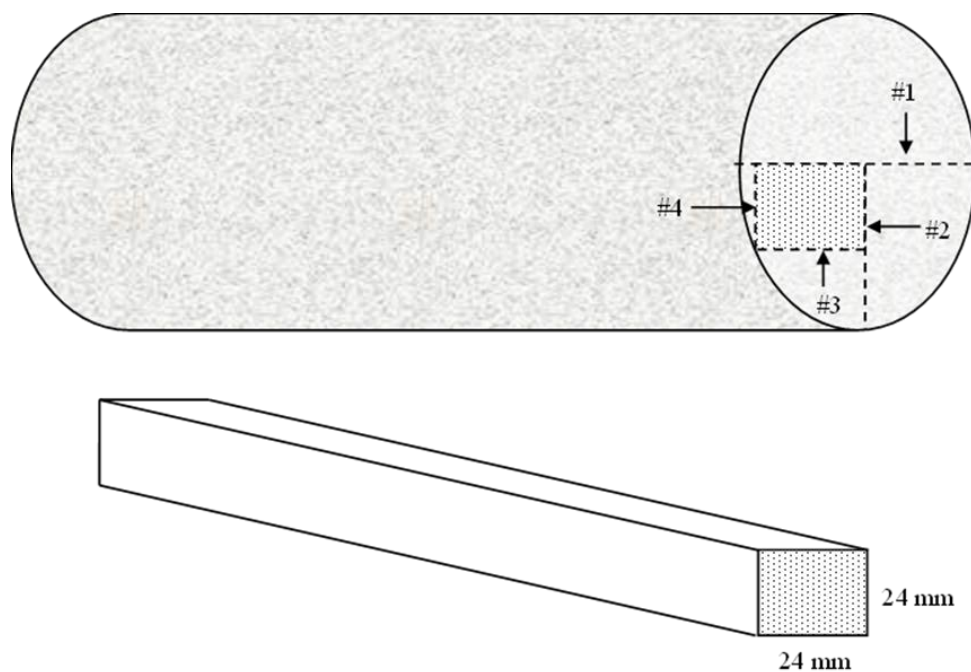


Figure 1. Ice core section and bandsaw cut locations (top), and chemical analysis stick with dimensions (bottom).

wrapped in clean plastic sleeves, and shipped frozen to the National Science Foundation – Ice Core Facility (NSF-ICF) in Denver, Colorado.

At NSF-ICF, SPC14 was prepared for chemical analysis as well as other measurements. Each core section was weighed to determine the density and was measured again for length to confirm depths measured during drilling. The ice cores were then cut lengthwise into sticks using band saws. The dashed lines in Figure 1 show the cut locations along the ice core to create the chemical analysis stick. For chemical analysis, each ice stick had dimensions of 24 mm x 24 mm x 1 m for use on a melter system (Winski *et al.*, 2019a). Once prepared, each chemical analysis stick was packaged in a clean sleeve to prevent contamination and sent to Dartmouth College in Hanover, New Hampshire for analysis.

2.2 Labware Cleaning Procedures

Before ice can be analyzed for chemical composition, all surfaces and labware that will come into contact with samples must be cleaned and tested to ensure each piece is contamination-free. This process uses ultrapure deionized water (for example: Milli-Q water purification system) to soak and rinse the labware; and the cleaned labware is allowed to dry in a clean air hood (Jauhiainen *et al.*, 1999, Osterberg *et al.*, 2006, Winski *et al.*, 2019a). This process ensures that the samples will also be free of contamination as they are processed for analysis.

Cleaning of labware (containers) and tools is typically performed by thorough washing with 18.2 megohm (M Ω) ultrapure deionized water. For labware, each piece is thoroughly rinsed three to five times with ultrapure water and allowed to air dry in a clean air hood. The clean air hood maintains a contamination-free atmosphere by filtering air

pulled through the hood. A positive pressure environment within the hood is created that keeps outside air from entering the hood to ensure only contamination-free air within the hood.

Each piece of labware is tested for contamination by replicating the analysis to be performed on ice samples with the ultrapure water. Since the ultrapure water and clean air hood are both free of contamination, each piece of labware is considered clean when the analysis shows no presence of any of the analytes of interest. For surfaces that will come into contact with the ice samples that cannot be tested in this manner, an ice blank is created from the ultrapure water. This ice blank is handled in the same manner as the ice stick/ice samples. The ultrapure ice stick/ice sample meltwater is collected in the same fashion as the samples. This meltwater is then analyzed to ensure no presence of contamination.

2.3 Sample Melting and Collection

After labware cleaning, a series of steps is used to prepare an ice stick into appropriate and contamination-free samples to be analyzed by instrumentation. This also requires dividing the ice stick lengthwise into individual samples. For SPC14, a continuous ice core melter system with a fraction collector was used to generate divided, contamination-free samples (Osterberg *et al.*, 2006).

Each ice stick was prepared by scraping each end with a pre-cleaned ceramic knife to remove any potential contamination at the end. After that, the ice stick was placed in a holder and melted on a heated metal melter with the temperature regulated by a controller; the holder and the melter were located in a stand-up freezer (Winski *et al.*, 2019a). The ice stick was kept centered on the melter via plastic tines (one for each side) (Winski *et al.*, 2019a). The melter was made of 99.9995% pure chemical-vapor-deposited silicon carbide

(Winski *et al.*, 2019a). The melter top is divided into an inner and an outer area. The inner section had dimensions of 16 x 16 x 3 millimeters which was high tiered and rimmed with tapered capillary slits that came together at a center drain hole (Winski *et al.*, 2019a). The outer area generated meltwater from the exposed surfaces (potential contamination) of the ice stick. The inner section construction prevents potential contamination from the meltwater generated in the outer section and wicking when melting porous firm (Winski *et al.*, 2019a). Figure 2 shows a schematic of the melter used for SPC14 (Osterberg *et al.*, 2006).

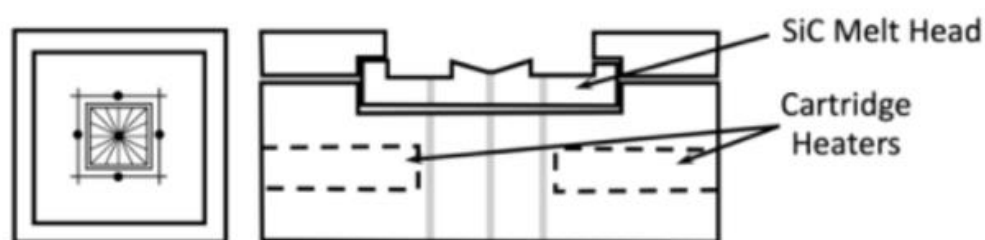


Figure 2. Melter schematic showing a top view (left) and side view (right).

The melter design depicted in Figure 2 allowed for a buffer of at least four millimeters between the outside of the ice stick and the edge of the inner section. A series of lines and a peristaltic pump were used to drain meltwater from the inner and outer sections of the melter. The inner section drains to a hole in the center and the contamination-free meltwater is pumped to a debubbler. Figure 3 shows a schematic of the entire sample collection setup (Winski *et al.*, 2019a).

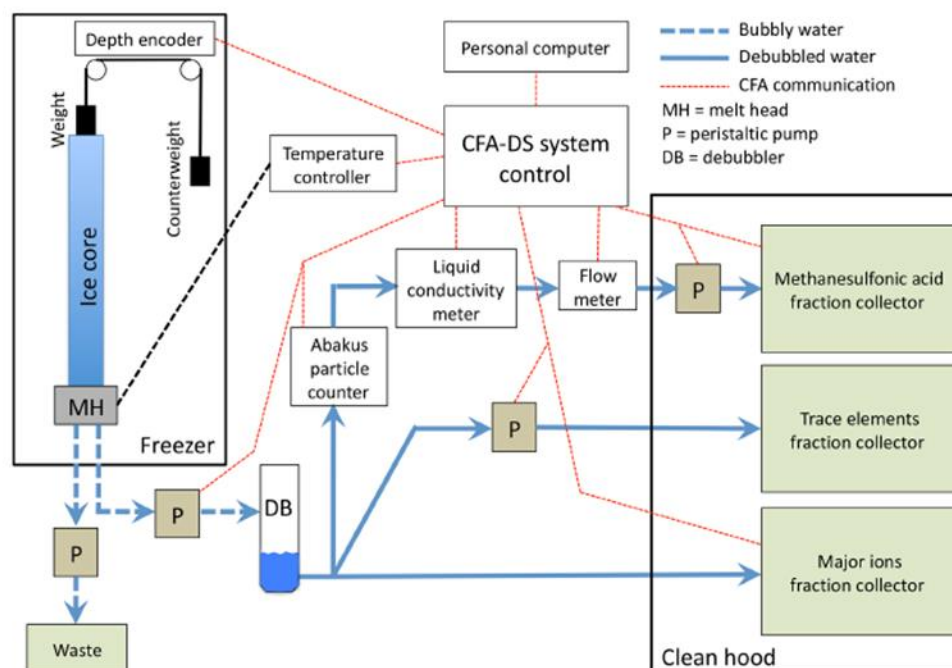


Figure 3. Schematic of continuous ice core melter system.

After air bubbles in the meltwater are removed at the debubbler, the meltwater stream was split with a splitter into three different fraction streams: one for major ion analysis, one for trace element analyses, and one that is measured for particles, liquid conductivity, and flow speed with a particle counter and size analyzer, an electrical conductivity meter, and a flowmeter (Winski *et al.*, 2019a). A Gilson FC204 fraction collector was used then used to collect samples from each of the split fractions. All samples were collected in clean vials, capped, and kept frozen until analysis (Winski *et al.*, 2019a).

2.4 Sample Depth Tracking

A size or depth interval must be assigned to each sample. This is paramount to dating an ice core (discussed later). For SPC14, this was accomplished during melting by using a software that utilized depth-point tracking developed by Breton *et al.* (Breton *et al.*, 2012). The software tracks each depth point in the ice stick as it travels through the

continuous melt analysis system right up to sample collection (Winski *et al.*, 2019a). By using the melt rates, flow rates, and line volumes, depths could be assigned to each sample. The assigned depths for the top and bottom of each ice stick are from the previously determined top and bottom depth of the tube, and the depth-point tracking system was used for the samples in between the two ends of the ice stick. For the Holocene (upper 800 m of SPC14), samples were collected every 1.1 centimeters on average (Winski *et al.*, 2019a).

2.5 Major Ion Analysis and Ion Chromatography

Samples collected for major ions were analyzed using a Thermo Fisher/Dionex ICS-5000 capillary ion chromatography system. This system consists of an autosampler, a pump, an injection valve, a separator column, a suppressor, a conductivity detector, and a computer (CPU). Figure 4 shows a schematic of the flow path through this system.

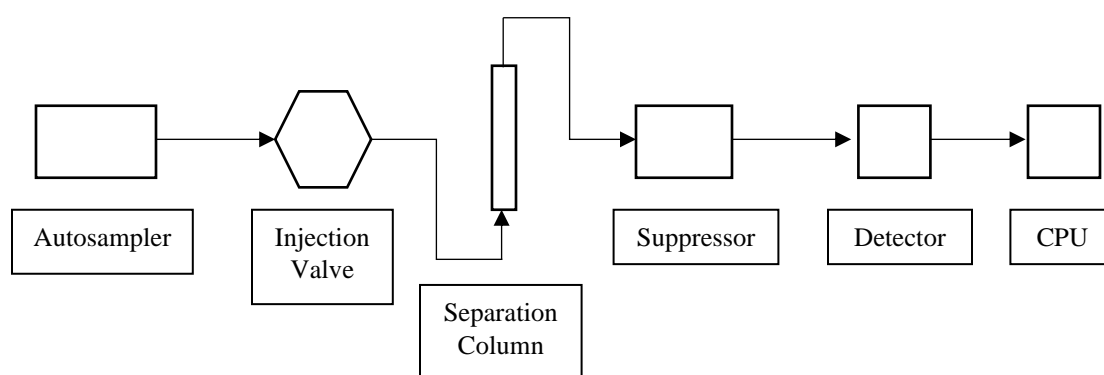


Figure 4. Ion chromatography system components and flow path.

This instrument was used to determine the concentrations of major anions (chloride, nitrate, sulfate) and major cations (sodium, potassium, magnesium, and calcium), quantified by linear calibration. Examples of the anion and cation chromatograms are shown in Figure 6 and Figure 5.

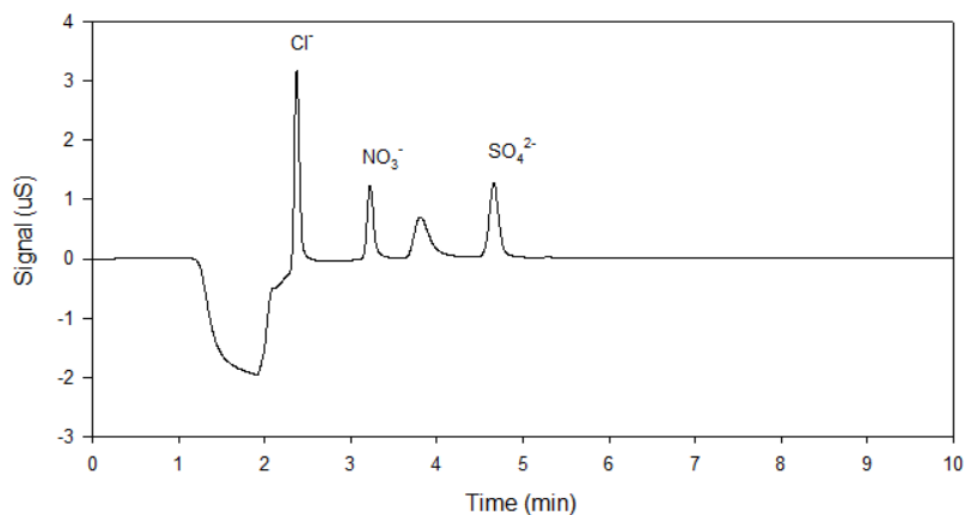


Figure 6. Anion chromatogram with retention times of chloride (Cl^-), nitrate (NO_3^-), and sulfate (SO_4^{2-}).

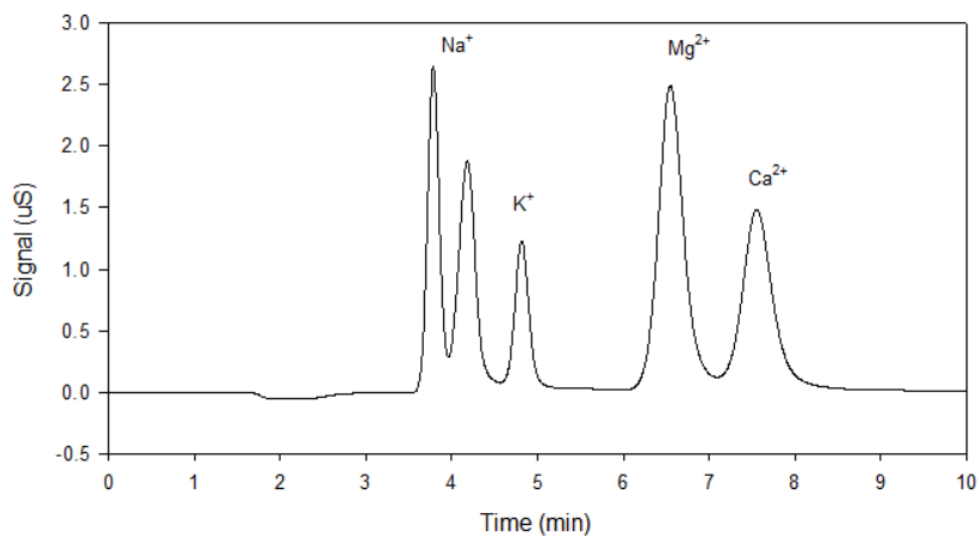


Figure 5. Cation chromatogram with retention times of sodium (Na^+), potassium (K^+), magnesium (Mg^{2+}), and calcium (Ca^{2+}).

One peak in each chromatogram is not labeled. The unlabeled peaks represent bicarbonate and ammonium in Figure 6 and Figure 5, respectively. While monitored, they were not quantified due to being easily contaminated during sample preparation and analysis via dissolution of carbon dioxide in solution and ammonium ions in laboratory air (Cole-Dai *et al.*, 2006, Legrand *et al.*, 1984).

2.6 Ice Core Dating

Depths were tracked throughout SPC14 via measurements made at the drill site, at core processing in NSF-ICF, and at the lab during sample analysis. The depth of each sample in an ice core must be converted to an age in order to create chronological records from ice cores. Since the concentrations of the major ions were also measured in each sample, both sample concentrations and depths can be used to date SPC14.

Graphs can be constructed that show the relationship between concentration of a chemical species and depth. The sodium concentration from SPC14 exhibits a distinct cyclic trend as shown in Figure 7.

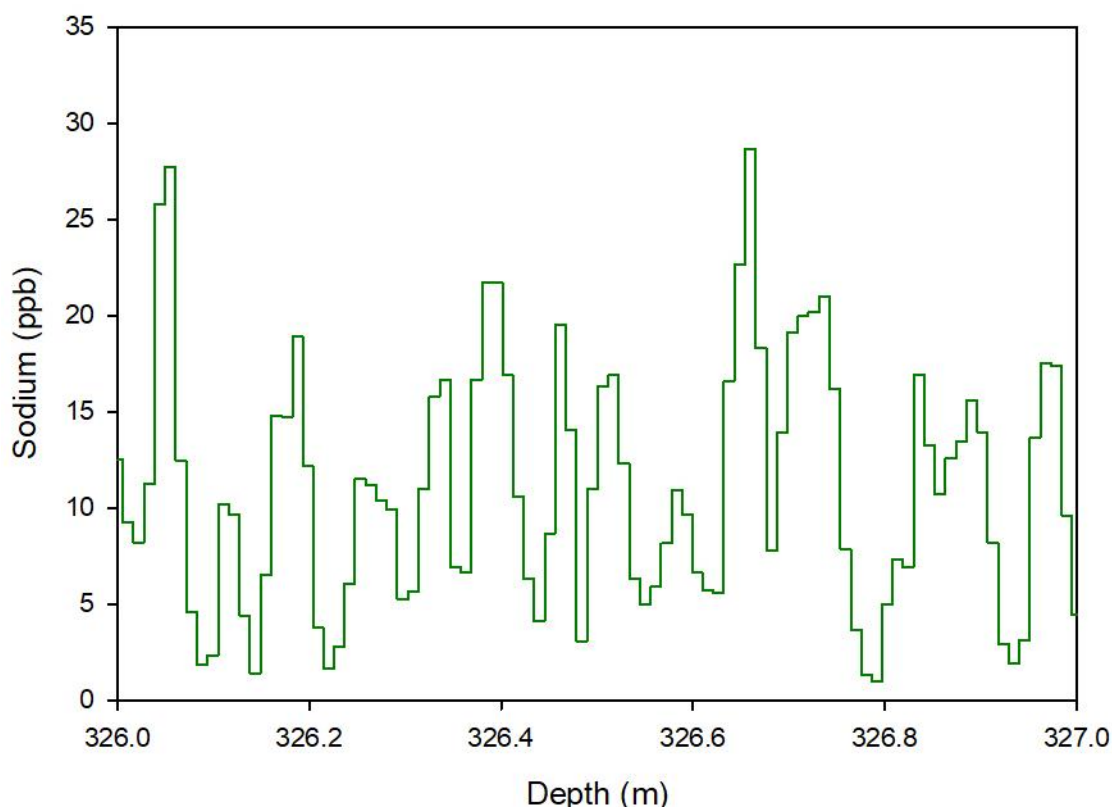


Figure 7. Cyclic variation of sodium from 326.0 m to 327.0 m.

The cyclical trend depicted in Figure 7 can be explained by understanding how the concentrations of major ions in snow change throughout the year. Sodium reaches a

relatively high concentration in winter snow due to strong winds bringing sea-salt to the drill site. In the summer, these winds are not as strong, and only small amounts of sea-salt are transported resulting in a low sodium concentration (Herron, 1982, Legrand and Delmas, 1984). The cyclical trend depicted in Figure 7 can then be thought of as seasonal cyclicity, where each peak-valley-peak cycle represents a year. As the chemical compounds in the atmosphere containing the major ions get trapped in accumulating snow, the seasonal cyclicity of these ions is recorded within snow layers. Since the snow accumulates in layers at the polar regions, the seasonal cycles can be used to determine the age of each snow layer, in a method called annual layer counting (ALC).

ALC takes advantage of the major ion seasonal cyclicity in the snow layers. For SPC14, sodium and magnesium were used for ALC due to clear and prominent annual cycles seen for both throughout the Holocene period. The age at a given depth can be determined by counting the number of annual cycles (concentration peaks) from the top of the core, and the distance (depth interval) between two peaks constitutes a year. In order to sufficiently resolve two distinct peaks, there must be a sufficient number of samples (sub-annual sample resolution) to see the oscillation within a year. Typically, six samples are the minimum number required when dating the ice core with ALC. For SPC14, sample sizes (depths) were approximately 1.1 cm. Using the data present in Figure 7, 14 years are present in the meter between 326.0 m and 327.0 m which leads to an average of 6.5 samples per year. For SPC14, the average samples per year at this depth yields an annual ice accumulation rate of 7.2 cm w.e. y^{-1} , consistent with the overall average accumulation rate of approximately 7.5 cm w.e. y^{-1} at the South Pole (Ferris *et al.*, 2011).

While ALC is an effective method to date an ice core, there are instances where its use is not feasible. As the depths get deeper in the ice core, the layers start to become thinner (smaller annual layer thickness or depth interval) due to the pressure of the ice above. At depths when there are an insufficient number of samples in a year, ALC may no longer be an effective method for counting layers. For SPC14, however, annual layers within the Holocene period were relatively thick, with respect to the sample size (1.1cm) to allow the use of ALC throughout this time period.

2.6.1 SP19 Dating Accuracy

The accuracy of ALC dating is not perfect, as seasonal cycles of a chemical species may not be always present and, occasionally, seasonal cycles are not well preserved in snow. Signals of events with known age or date of occurrence can be used to improve the dating accuracy of an ice core. These known events are referred to as stratigraphic time markers and are defined as well-documented past atmospheric perturbations (Legrand and Mayewski, 1997). In addition to ALC, the WAIS Divide timescale (WD2014) used some stratigraphic time markers to date the WAIS Divide ice core (WDC) to improve dating accuracy (Sigl *et al.*, 2016). The final SPC14 timescale (SP19) was developed using ALC along with prominent volcanic events identified in WDC (Winski *et al.*, 2019a). SP19 used the WD2014 dates of these volcanic time markers to verify or correct the ALC-determined dates of these events in SPC14. These markers in WD2014 and SP19 are referred to as volcanic tie points. For this work, these volcanic tie points offer a way to improve the accuracy of ALC.

ALC offers a robust way of discerning years in an ice core; however, this dating method is still subject to error. Two main causes of errors in ALC are: 1) the ability of the

snow accumulation to preserve the seasonal variations, and 2) incorrect identification of the annual layers that are preserved in the records (Sigl *et al.*, 2016). The WD2014 timescale is demonstrated (Sigl *et al.*, 2016) to be very accurate. As a result, the age of the signal of a volcanic event in SP19 can be accurately determined if the signal of the same eruption is located in the WD2014. This age from WD2014 can be a check on the accuracy of the ALC-dated age of the signal in SP19. The use of 251 volcanic tie points (80 in the Holocene) improved the accuracy of SP19 (Winski *et al.*, 2019a). Figure 8 shows an example of a tie point (red dot) in both SP19 and WD2014 using a volcanic event which was known to occur in 1815 CE.

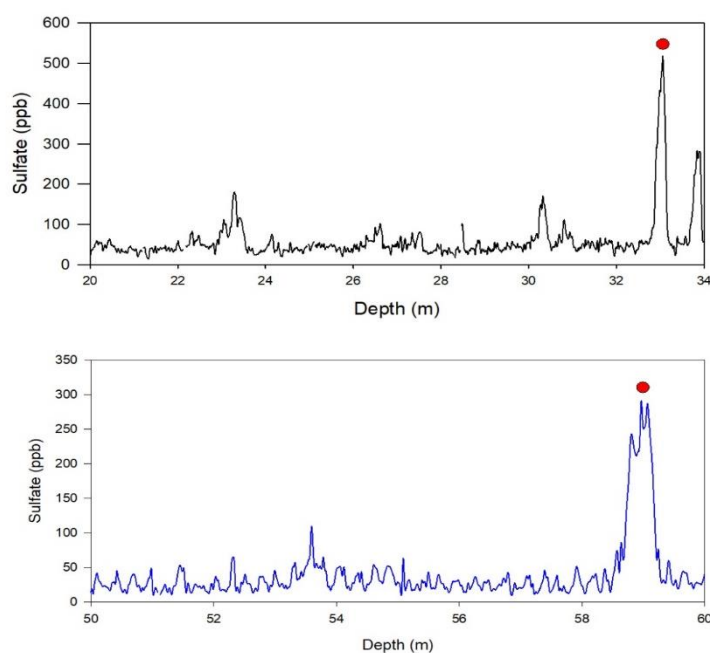


Figure 8. Volcanic tie point in SP19 (top, black) and WD2014 (bottom, blue).

While the 1815 CE event is visible in both cores, they occur at different depths. In WD2014, the 1815 CE event appears at approximately 59 m; and in SP19 it appears at approximately 33 m. This difference in depth can be attributed to the higher snow

accumulation rate at WAIS Divide ($\sim 20 \text{ cm w.e.}\cdot\text{y}^{-1}$) than that at the South Pole ($\sim 8 \text{ cm w.e.}\cdot\text{y}^{-1}$). The SP19 dating accuracy is improved because as a volcanic tie point is reached, a certain number of years must be counted in ALC. This requires that the number of years between two tie points be adjusted if ALC yields either a high or low number of years in SPC14.

The SP19 dating accuracy was assessed with respect to the WD2014 timescale by using the difference between the number of ALC-determined years in a known 500-year period. This assessment showed that the maximum error of ALC dating for SPC2014 is 6.7%.

2.6.2 SP19 Dating Uncertainty

While the accuracy of the SP19 timescale can be improved by the process stated in section 2.6.1, the precision, or uncertainty, of the timescale must be considered as well. Uncertainty occurs when instances arise where an annual layer may be difficult to distinguish as one layer or two layers. The SP19 dating uncertainty was assessed with respect to the WD2014 timescale by using the drift from counting years among different interpreters. Different interpreters are used to determine points where ambiguities may arise from the counting of individual years.

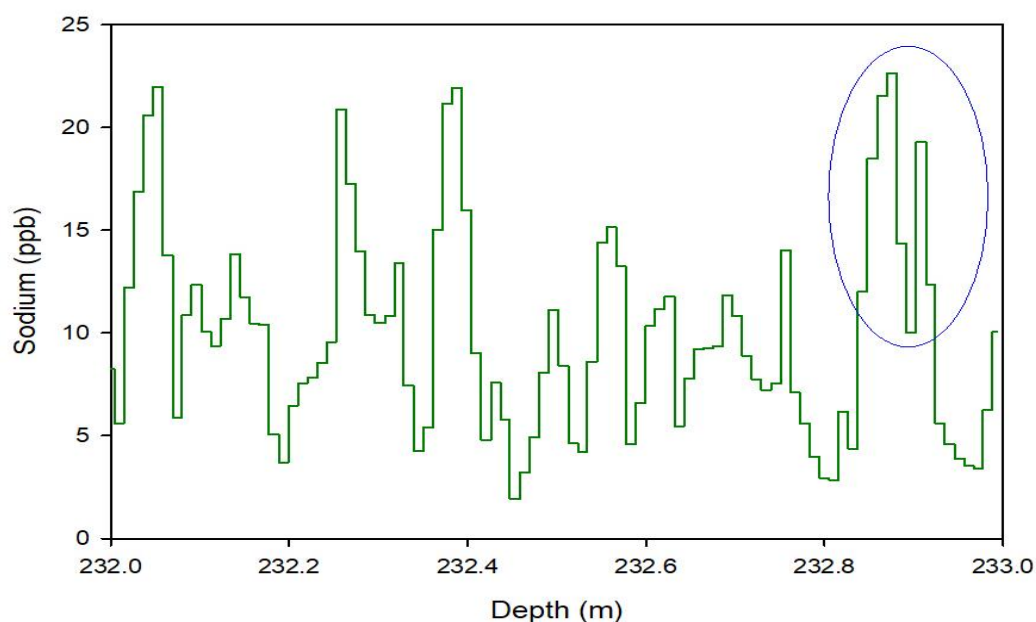


Figure 9. ALC precision example from SP14 using sodium from 232.0m to 233.0m. Blue circle indicates a potentially uncertain year.

Figure 9 shows an example where identification of a year may be uncertain. The blue circle shows a point where two peaks are very close together. In these instances, one interpreter may count two peaks, and a different interpreter may only count one peak. The first interpreter may interpret that the snow accumulation rate during this time is low leading to the small depth interval (annual layer thickness) between the two peaks. However, the other interpreter may view that the peak on the right may be caused by irregular or unusual deposition of sodium and is not an annual peak. Such differences in annual layer identification during data interpretation result in uncertainty of dating (number of years counted). For sections of SPC14 that have large depths between tie points, the uncertainty of the timescale results from different decisions on if and how ambiguous layers are counted.

Five different interpreters independently counted the number of years over 500-year intervals in the final SP19 synchronized timescale (Winski *et al.*, 2019a) to determine the uncertainty from the differences in counting between interpreters.

Since the SP19 chronology is anchored to WD2014 via volcanic tie points, the total uncertainty of the final SP19 timescale must account for both the uncertainty attributed to WD2014 and the uncertainty between the volcanic tie points in SP19. A volcanic tie point zeros out the uncertainty at the age of the tie point in SP19. However, there is still uncertainty in the age in SP19, since uncertainty (of the tie point itself) also exists in WD2014. The overall uncertainty at any age in SP19 is the combined uncertainties of ALC in SP19 and WD2014. The overall uncertainty in SP19 is calculated by using a root sum of squares of the WD2014 timescale and the interpolation between volcanic tie points from SP19. The plot in Figure 10 shows the uncertainty attributed to the WD2014 (light blue area), the interpolation uncertainty in SP19 using the volcanic tie points (blue line), and the total uncertainty from the root sum of squares (black line) (Winski *et al.*, 2019b).

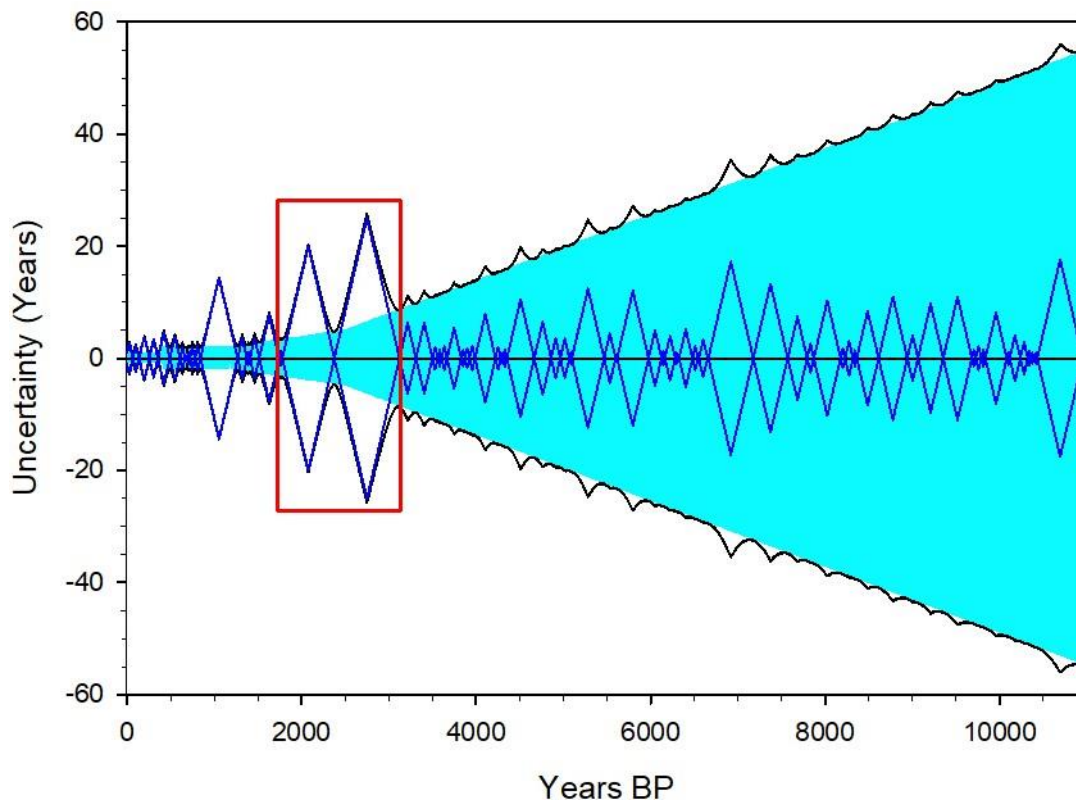


Figure 10. SP19 timescale uncertainty determination during the Holocene. Light blue area represents WD2014 uncertainty, blue line represents SP19 uncertainty, and black line represents total uncertainty in SP19. Red box indicates portions of largest uncertainty between volcanic tie points in SP19.

Figure 10 shows that the WD2014 uncertainty (light blue area) increases steadily further back in time, reaching maximum of ± 55 years. The largest uncertainty between volcanic tie points in SP19 reaches a maximum of approximately ± 25 years between 1800 and 3100 years BP (red box); however, the rest of the SP19 uncertainty does not exceed ± 18 years (Winski *et al.*, 2019a). The total uncertainty for the SP19 timescale reaches a maximum of ± 55.1 years, found at the beginning of the Holocene (Winski *et al.*, 2019b).

2.7 Sources of Sulfate in Antarctic Snow

Graphs of sulfate can be made similar to that of sodium which show how the concentrations change as a function of depth or time (Figure 11).

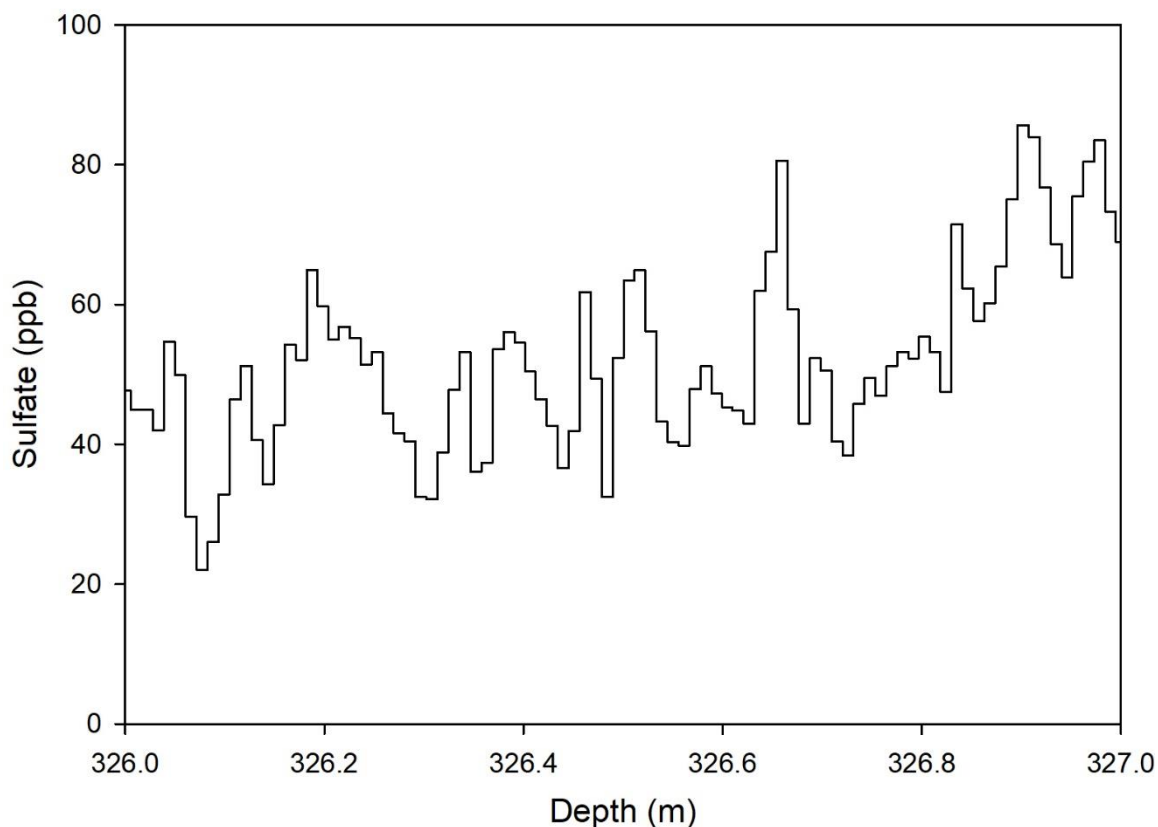


Figure 11. Cyclic variation of sulfate in SP14 from 326.0 m to 327.0 m.

However, the measured (total) sulfate consists of sulfate from three sources: sea-salt, marine biogenic emissions, and volcanic eruptions (Delmas, 1982). Anthropogenic sources of sulfate in Antarctic snow are considered to be negligible due to being surrounded by oceans (Legrand and Mayewski, 1997). To determine the amount of sulfate solely from volcanic eruptions, sulfate from sea-salt and marine biogenic sources must be removed from the total sulfate.

Sea-salt sulfate can be accounted for by using the ratio of sulfate concentration to sodium concentration ($\text{g}\cdot\text{kg}^{-1}$) in bulk seawater, and this ratio is 0.2515 (Millero *et al.*, 2008). This ratio along with the sodium concentration in each sample is used to calculate

non-sea-salt sulfate (nss-sulfate or nss-SO₄²⁻), seen in Equation (1) (Kirchner and Delmas, 1988).

$$[nss - SO_4^{2-}] = [SO_4^{2-}] - (0.2515 \times [Na^+]) \quad (1)$$

Nss-sulfate is therefore made of sulfate only from marine biogenic emissions and volcanic eruptions. Marine biogenic sources are attributed to dimethylsulfide (DMS) emissions which are usually oxidized to sulfate in the atmosphere. Marine biogenic sulfate is the natural background as DMS emissions are continuous. During volcanic eruptions, volcanic sulfate is superimposed on this background. This is important as volcanic sulfate, which is related to the magnitude of volcanic eruptions, can be calculated from the nss-sulfate and the natural background sulfate.

2.8 Sulfate Flux

Concentrations alone do not consider the effects of varying snowfall accumulation. For example, one year may have a high accumulation and the next year may have very little. If the same amount of sulfate by mass was deposited each year, the high accumulation year would have a low sulfate concentration due to a greater volume. Correspondingly, the year with little snow accumulation would have a high sulfate concentration. Since snow accumulation rates vary from year to year, variations in sulfate concentrations may be caused by the varying snow accumulation, rather than by the amount of sulfate in the atmosphere, which is the desired quantity. Thus, a different parameter than concentration is needed to represent the amount of sulfate in snow and in air.

One parameter that considers the amount of mass falling on or entering to a given area is called flux. Depositional flux is defined as the mass of a chemical substance deposited over a given area in a certain amount of time (Kennedy, 2020):

$$Flux = \frac{mass}{area \times time} \quad (2)$$

Time for an ice core can be left out of Equation (2) since the length or depth interval of each sample corresponds to a length of time to determine annual totals. Mass needs to be calculated from the sulfate concentrations (reported in micrograms per liter) and the volume of the meltwater sample, which requires the water equivalent volume for each sample. Since the cross-sectional area and length of each sample is known, Equation (3) can be used to find the volume in water equivalent for each sample.

$$volume\ in\ water\ equivalent = area \times sample\ size \quad (3)$$

The sulfate flux can then be calculated using the volume in water equivalent in Equation (3) via the following:

$$Sulfate\ Flux = [SO_4^{2-}] \times sample\ size\ (w.e.) \quad (4)$$

Sample size (depth interval) was tracked as samples were collected for analysis; however, sample size is measured from the depth interval in the ice core, while the sample size used to calculate the volume must be that of the meltwater (water equivalent), which is equal to the sample size multiplied by the density of the sample.

Density is not uniform throughout the ice core. Loosely packed snow with low density is found at the top of the ice core, and as the snow becomes more packed at depth,

the density increases. This is why the density of samples towards the top of the ice core is lower than those found at deeper depths.

The volume (length and diameter) and mass of each one-meter ice core section are usually measured during drilling, and the density of each section is subsequently calculated (Graeter *et al.*, 2018). The density so calculated is the average density of the one-meter section. To compute the mass flux of each sample, the density of the sample is needed. In practice the measured densities are plotted against depth, and a best-fit function is obtained from the data which allows for the determination of density by calculation at any depth in the ice core (Cole-Dai *et al.*, 1997). Sample flux can then be calculated by multiplying the sample sulfate concentration by the sample size in water equivalent. The flux of all samples that make up a given year can then be summed together to yield the annual sulfate flux – the total mass of sulfate deposited over a unit area per year.

2.9 Ice Sheet Thinning Consideration

While the average accumulation rate represented by layer thickness has been previously discussed, the layer thickness does not remain the same when the layer is being buried to depth. South Pole layer thicknesses are affected by three factors: 1) surface accumulation spatial variability; 2) snow accumulation affected by changes due to past climate-related changes; and 3) ice flow causing post-depositional thinning (Lilien *et al.*, 2018). The third point can be accounted for via a modeled thinning function. Thinning functions, such as the Dansgaard-Johnson model (Dansgaard and Johnsen, 1969), are defined as the fractional amount of thinning that has occurred at a given depth in the ice sheet (Kahle *et al.*, 2021).

The SP19 timescale used the Dansgaard-Johnson model to estimate the amount of thinning for each layer of ice (Winski *et al.*, 2019a). The model yields a thinning correction factor for each year in the SP19 timescale. The thinning correction factor (F) ranges from 1.00 at the top of the ice core to 0.71 at the beginning of the Holocene. The factor was used in this work to amend the flux calculated from measured concentrations and water equivalent sample sizes to account for the thinning at deeper depths in the ice core by dividing the flux value for a given year by the correction factor, F.

3. RESULTS

3.1 SPC14 Sulfate Flux Dataset

The annual nss-sulfate flux values can be plotted against time in years before present (years BP, present being 1950 CE) to create SPC14 volcanic record through the Holocene in Figure 12.

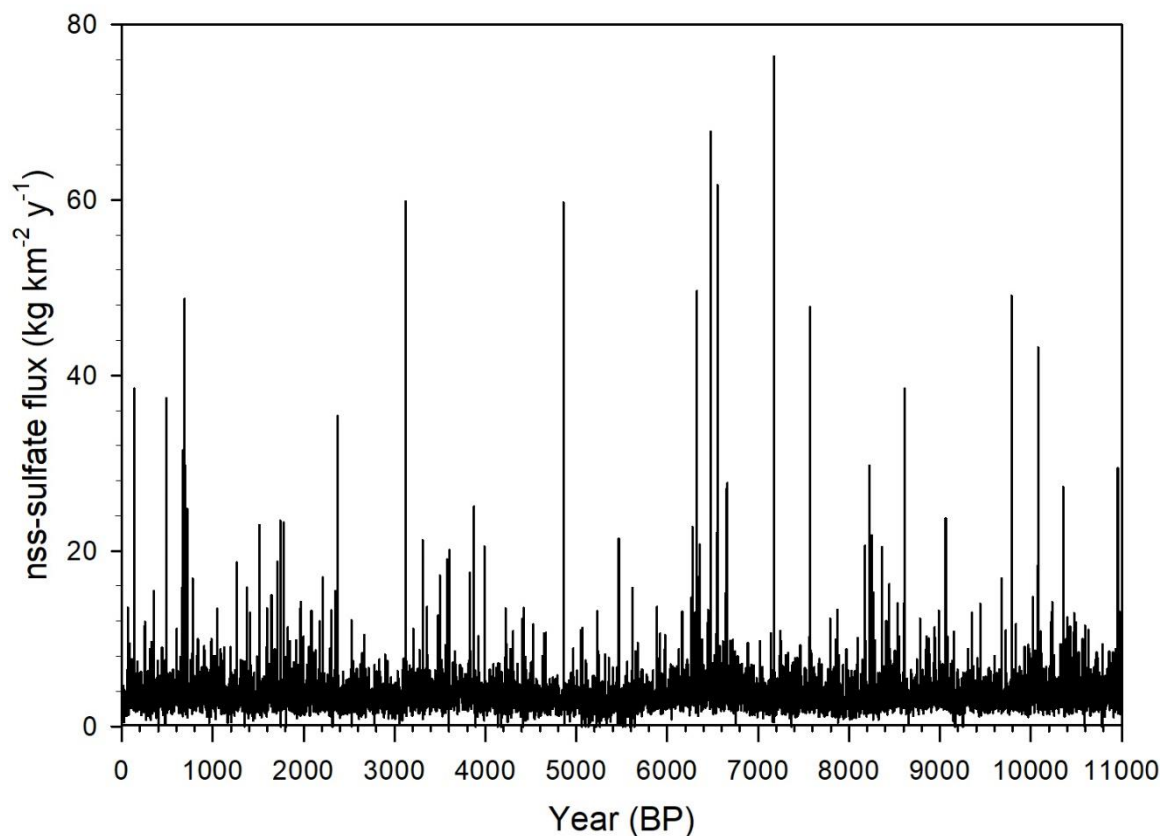


Figure 12. Annual non-sea-salt sulfate flux in the Holocene for the SP14.

The SPC14 sulfate flux profile shows a distinct baseline is present with numerous large nss-sulfate flux values lasting a year or a few years. The large values are most likely years when volcanic eruptions took place and are therefore signals of volcanic events. Very large signals are readily identifiable against a low, but fluctuating, baseline (approximately $6-9 \text{ kg}\cdot\text{km}^{-2}\cdot\text{y}^{-1}$). However, nss-sulfate flux values that are close to the baseline are harder

to determine if they represent volcanic events or if they are just a part of the fluctuating background or baseline. To determine if these are volcanic events, it is necessary to define the level of the background and its range of fluctuation, which would lead to the upper limit of the background and consequently a detection threshold for volcanic signals.

3.1.1 SPC14 Volcanic Detection Threshold

Usually, the mean or average of all data points in a dataset with varying values can represent the typical data value in the dataset. As most data values in the sulfate flux dataset are from the background, we could assume that the mean represents the background. One parameter for quantifying the range of the background is the standard deviation. Therefore, we may define the upper limit with a 95% confidence interval by using the mean plus two times the standard deviation ($\bar{x} \pm 2\sigma$). This would establish the detection threshold for volcanic event signals in the dataset. This approach assumes that the background sulfate flux in South Pole snow is constant over the period covered by the dataset. However, the background level is not constant.

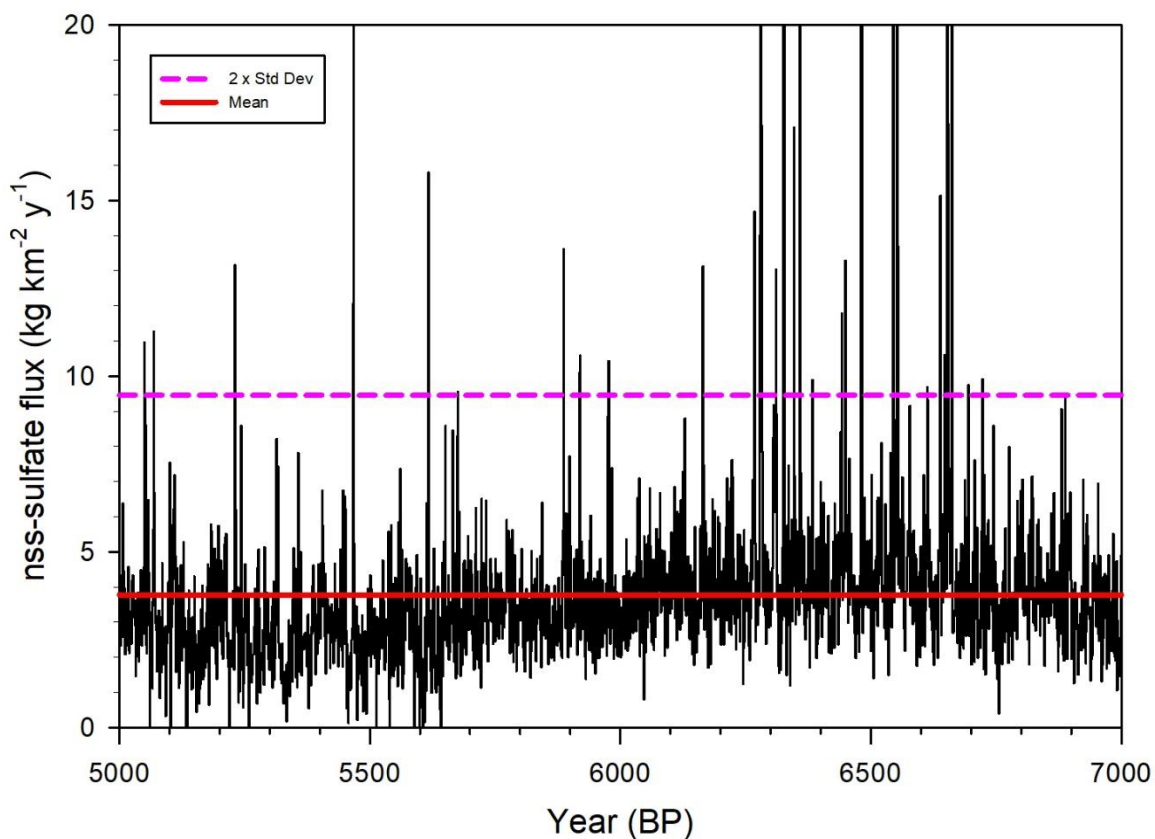


Figure 13. Magnified view of SP14 nss-sulfate flux data with mean as the non-volcanic background and mean plus two times the standard deviation as the threshold.

Figure 13 shows how the mean does not accurately represent the background for the SPC14 sulfate flux dataset. Between the years 5000-6000 BP, the background sulfate flux levels slowly decrease and then begin to increase. The opposite is seen between 6000-7000 BP where the values increase and then decrease. In addition, the mean value is influenced by the very large sulfate flux values found throughout the Holocene period. This type of method shows that an accurate detection threshold needs to take into consideration: 1) the large sulfate flux values influenced by volcanic eruptions and 2) the fluctuations in background flux.

One method for addressing the influence of the large volcanic-affected sulfate flux values is to use the median instead of the mean, which would minimize the influence of the relatively few large sulfate flux values. To address the fluctuating background flux a running median (RM) can be used. A RM is similar to a moving average in that a median is found for a subset of the data, or window (a period of time in this case), which can be moved throughout the dataset. For SPC14, a running median with a 41-point (41-year) window (41-pt RM) was used to create a variable background seen in Figure 14.

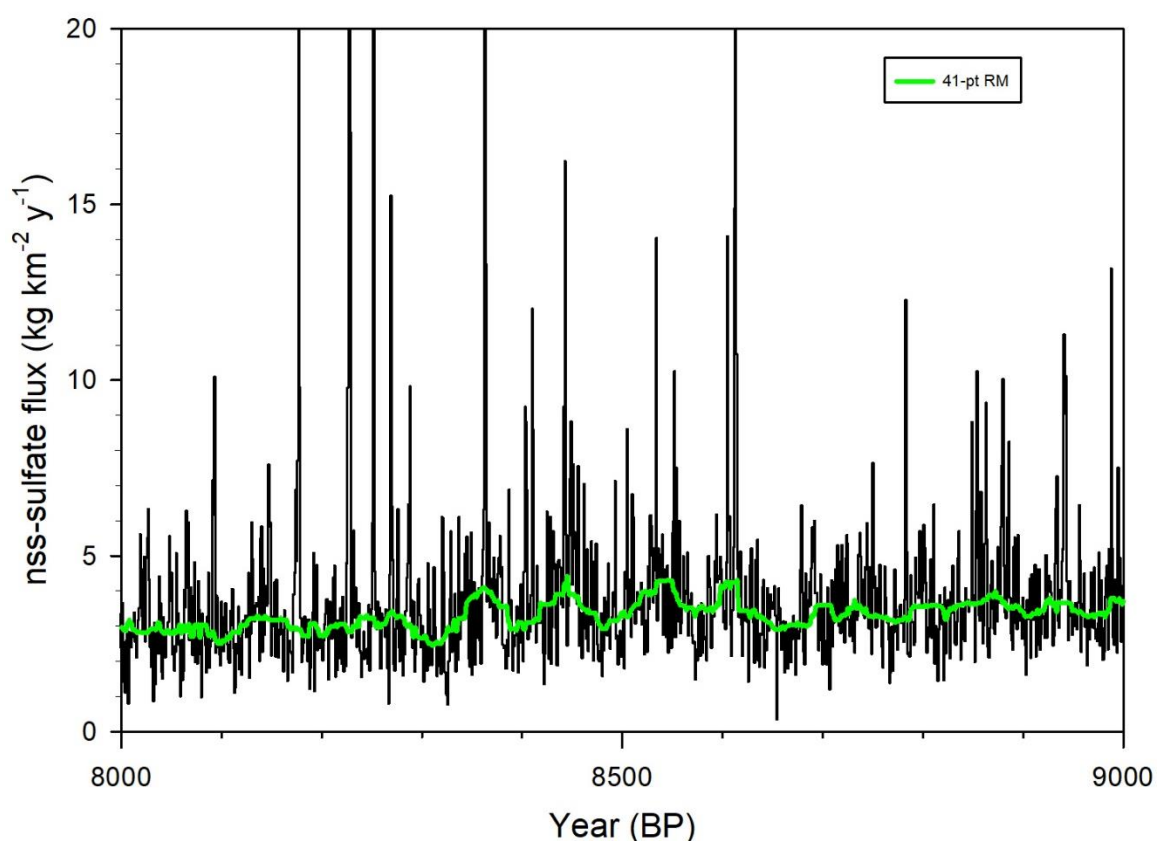


Figure 14. SP14 volcanic record with 41-pt RM.

The 41-point RM creates smoothed-fit line for SPC14 background sulfate flux. As seen in Figure 14, the RM is able to fit the fluctuations in the flux values and to reduce the influence of the very large flux values. In order to create a detection threshold, a value is

needed to assess the variability of the median values. We selected the median absolute deviation (MAD) which is defined in Equation (5) (Zach, 2022),

$$MAD = \text{median}(|x_i - x_m|) \quad (5)$$

where x_i is the i^{th} value in the dataset (medians of all 41-point windows) and x_m is the median value of the dataset. Using MAD, the detection threshold, y_t , can then be defined as follows:

$$y_t = RM + k(MAD) \quad (6)$$

where k is the threshold adjustment parameter. A previous study empirically selected the threshold adjustment parameter as $k = 4$ which was suited for volcanic event detection in a nss-sulfate record from an Antarctica ice core (Traufetter *et al.*, 2004). Using Equation (6) the SPC14 detection threshold can be applied to the SPC14 dataset as shown in Figure 15.

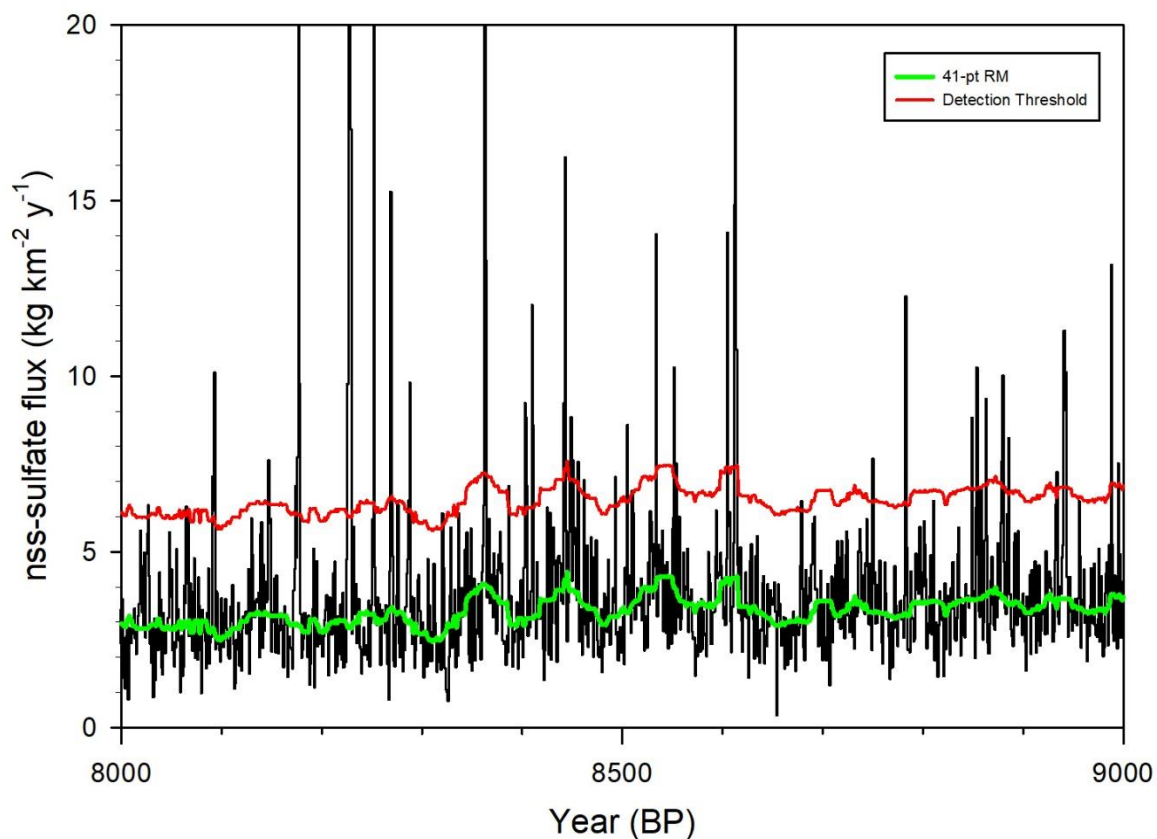


Figure 15. SP14 RM and detection threshold for 8000-9000 BP.

The effect of the window size was investigated in a study of the volcanic events at WAIS Divide (Cole-Dai *et al.*, 2021). The WAIS Divide study investigated window sizes of 31, 41, and 51 years. While the number of events detected by the large window did not differ significantly from the 41-year window, the small window generated 43 additional volcanic events. However, these additional volcanic events did not have very large volcanic flux values, with the largest of these additional events being no more than 10% of the volcanic flux of Tambora (Cole-Dai *et al.*, 2021). This led to the use of the 41-year window for the detection threshold in this work.

3.1.2 SPC14 Sulfate Background

The 41-point RM and threshold can now be used to determine the natural sulfate flux background. This is done by removing all the volcanic events above the detection threshold, seen in Figure 16.

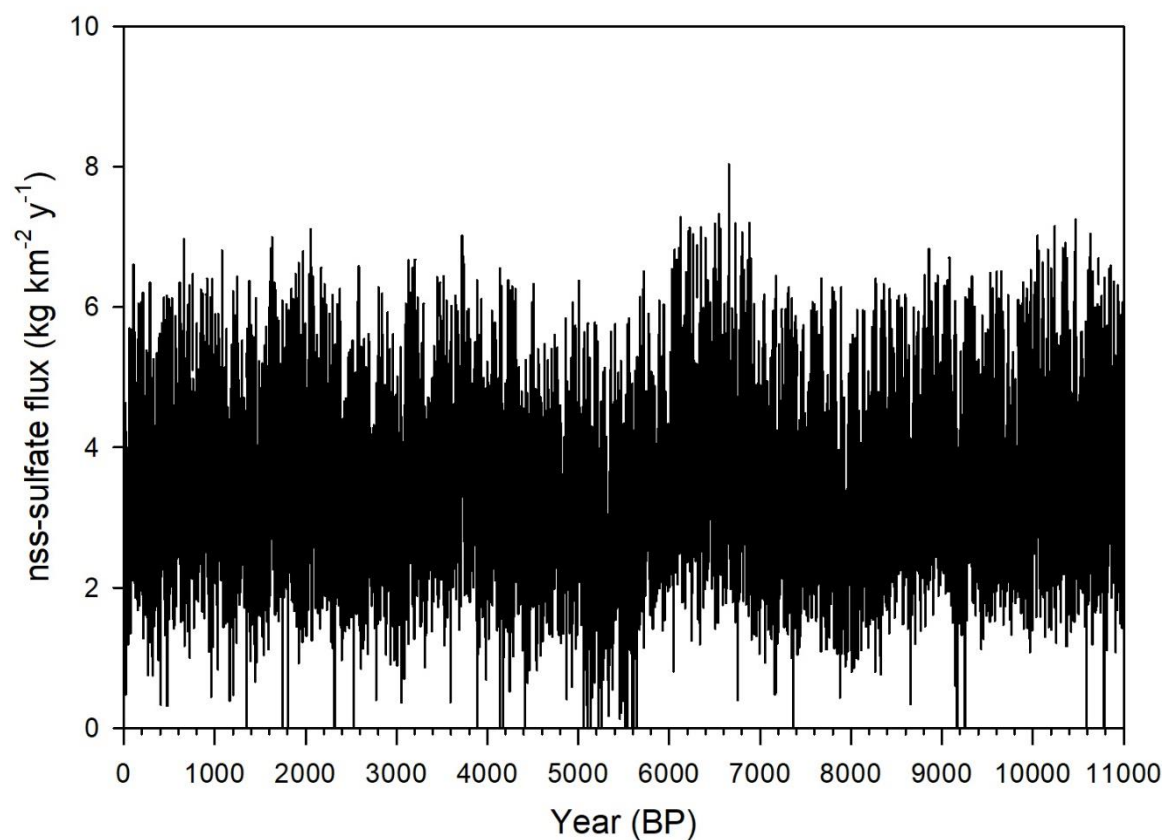


Figure 16. SP14 background nss-sulfate after removal of volcanic events.

The background nss-sulfate flux level is important in determining the flux of volcanic events in the record. Since all the volcanic events have been removed from the sulfate flux record, a running mean can be applied to the data. Using the same 41-point

running window, the reduced running mean (RRM) generates the background nss-sulfate flux for SPC14, with a 1000-year magnified view shown in Figure 17.

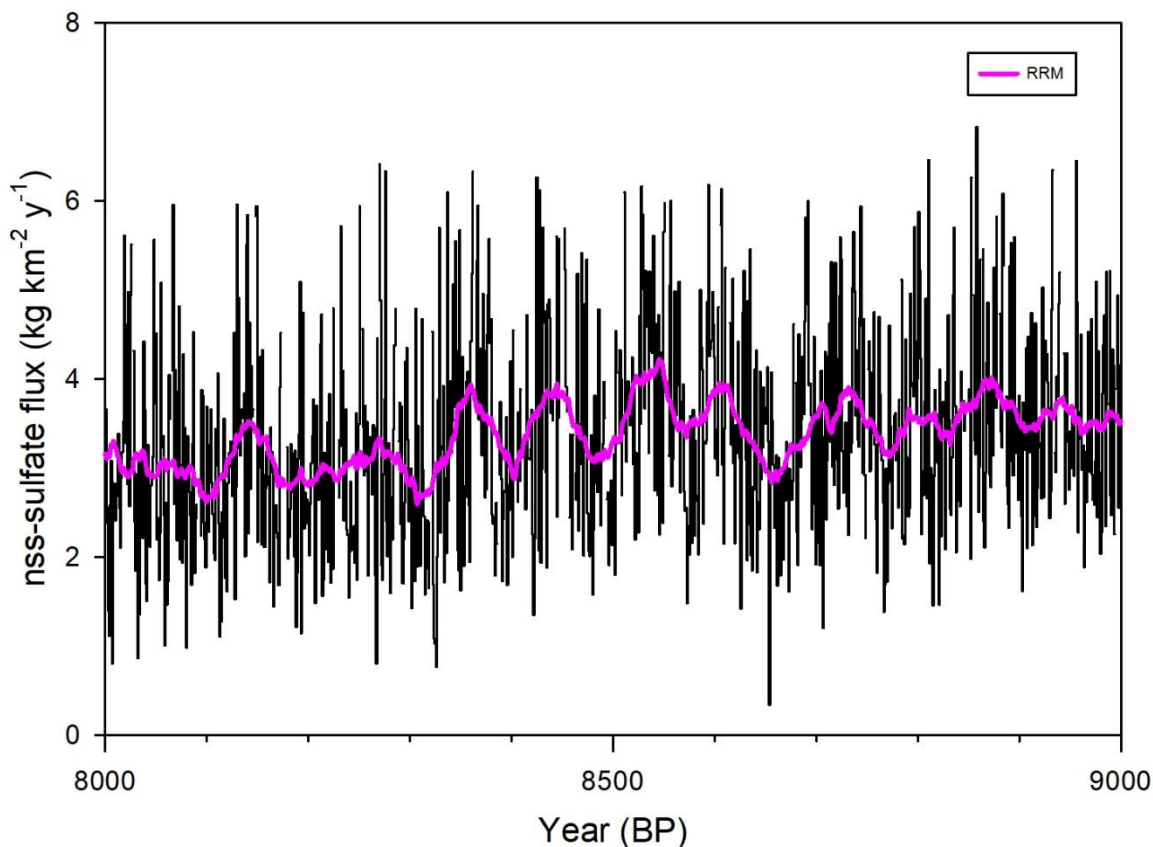


Figure 17. Background nss-sulfate w/RRM from 8000 to 9000 years BP.

3.2 Volcanic Flux of Volcanic Events

Years in the SPC14 sulfate flux dataset with sulfate flux values above the detection threshold in Figure 15 can now be considered to contain volcanic sulfate. The nss-sulfate background is needed to calculate the volcanic flux of a year in SPC14. Volcanic flux is defined as the difference between the total nss-sulfate flux and the non-volcanic background represented by the RRM. The volcanic flux can be used to estimate the climate forcing of a volcanic eruption. Since the signal of major volcanic eruptions can last for more than one year, consecutive years with volcanic flux values exceeding the threshold

and considered one event. Volcanic flux of all years in an event is summed to yield the total volcanic flux of that event. Table 1 shows an example of the volcanic flux for two events from a period between 1805 and 1820 CE.

Table 1. Volcanic flux event examples.

Year (BP)	Actual Year (CE)	Corrected Annual SO ₄ ²⁻ Flux (kg·km ⁻² ·y ⁻¹)	Threshold RM + (4 x MAD) (kg·km ⁻² ·y ⁻¹)	Reduced Running Mean (RRM) (kg·km ⁻² ·y ⁻¹)	Values Above Threshold (kg·km ⁻² ·y ⁻¹)	Volcanic Flux (kg·km ⁻² ·y ⁻¹)
130	1820	1.86	6.56	3.36		
131	1819	4.40	6.56	3.31		
132	1818	2.92	6.39	3.29		
133	1817	4.92	6.37	3.25		
134	1816	17.10	6.33	3.16	17.10	13.94
135	1815	38.51	6.37	3.18	38.51	35.33
136	1814	8.34	6.37	3.18	8.34	5.16
137	1813	2.77	6.37	3.18		
138	1812	2.22	6.28	3.15		
139	1811	6.35	6.08	3.13	6.35	3.22
140	1810	8.25	6.28	3.24	8.25	5.01
141	1809	26.03	6.28	3.24	26.03	22.79
142	1808	2.75	6.28	3.22		
143	1807	3.23	6.37	3.30		
144	1806	2.08	6.39	3.32		
145	1805	3.69	6.39	3.33		

Table 1 shows how the volcanic flux is determined for two events: an event with a start year of 1809 and the second with a start year of 1814. Each event lasts for three years, and the total volcanic flux for the 1809 event is 31.02 kg·km⁻² and the 1814 event is 54.43 kg·km⁻². All events are designated by the first year they appear in the ice core chronology.

For SPC14, 416 events were identified and total volcanic flux was obtained using the method described above. This produced a list of all events with volcanic flux which is

referred to as the *2022 SPICEcore Holocene Volcanic Record, SPVR2022*. The SPVR2022 record of all 416 events is found in Appendix A.

3.3 Frequency of Events

When the 416 events are grouped by millennium, an average of 37.8 events is found per millennium, as depicted in Figure 18.

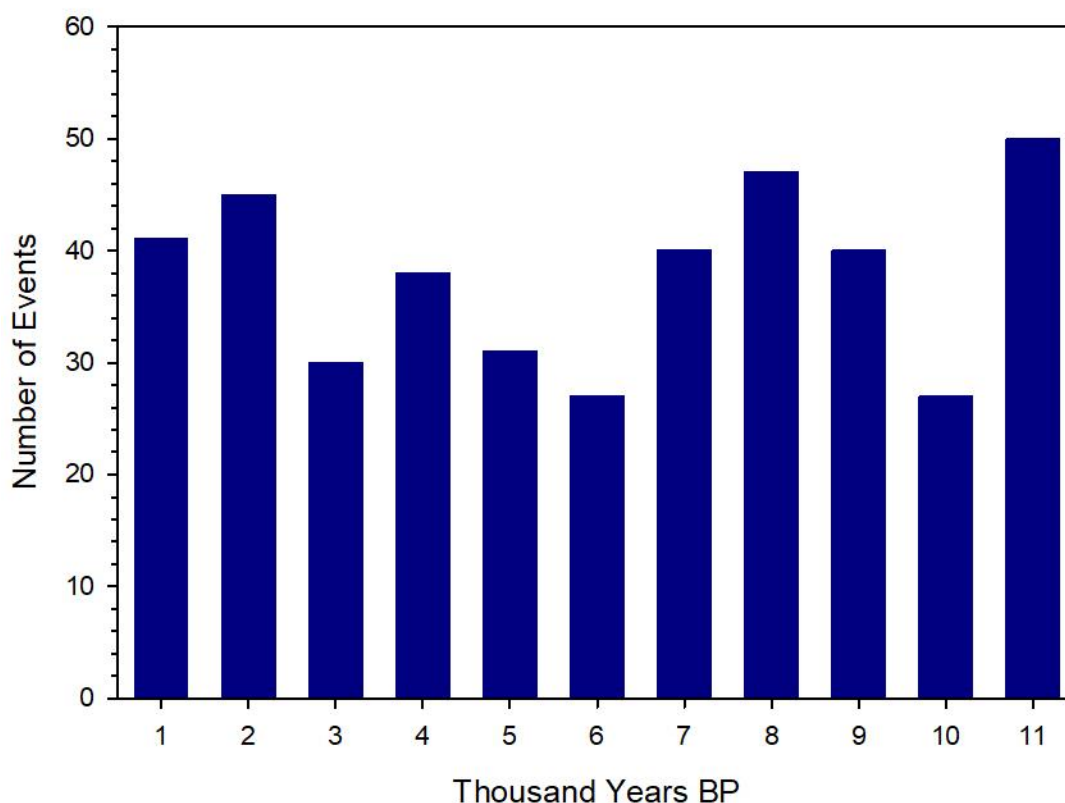


Figure 18. Number of events by millennium in SPC14.

The frequency of events is highest at the beginning of the Holocene, with 50 events identified in the eleventh millennium (10 ka-11 ka years BP). The rest of the Holocene does not show any distinct trend with ranges from a high of 47 events in the eighth millennium and to a low of 27 events in the sixth and tenth millennia.

3.4 Largest Events by Volcanic Flux in SPVR2022

The 416 events in SPVR2022 are all considered large events with the potential to impact global climate. The largest events by volcanic flux during the Holocene are displayed in Table 2.

Table 2. Ten largest events by volcanic flux in SPVR2022.

Event Number	Year BP	Year CE	Total Volcanic Flux $\text{kg}\cdot\text{km}^{-2}$	Duration Year
260	7177	-5227	110.58	2
183	4860	-2910	104.21	3
221	6328	-4378	100.37	4
230	6482	-4532	93.05	3
234	6554	-4604	88.59	4
121	3124	-1174	79.6	4
360	9790	-7840	78.38	3
280	7572	-5622	76.27	4
27	692	1258	71.51	2
370	10082	-8132	68.12	4

The average duration for each of these events is 3.3 years, indicating the strength of the volcanic forcing of the largest events in SPVR2022. These large events have no apparent trend over the course of the Holocene, but seven of the largest events took place during the first half of the Holocene (5000 to 10,000 years BP). The most recent event in this list would be Event Number 27 which occurred in the year 1258 CE. This event is attributed to the 1257 eruption of Mount Samalas located in Indonesia, one of the largest stratospheric eruptions during the Common Era which may have cooled the planet for a period of time during the 13th century (Vidal *et al.*, 2016).

3.5 Event Comparison Using Volcanic Flux

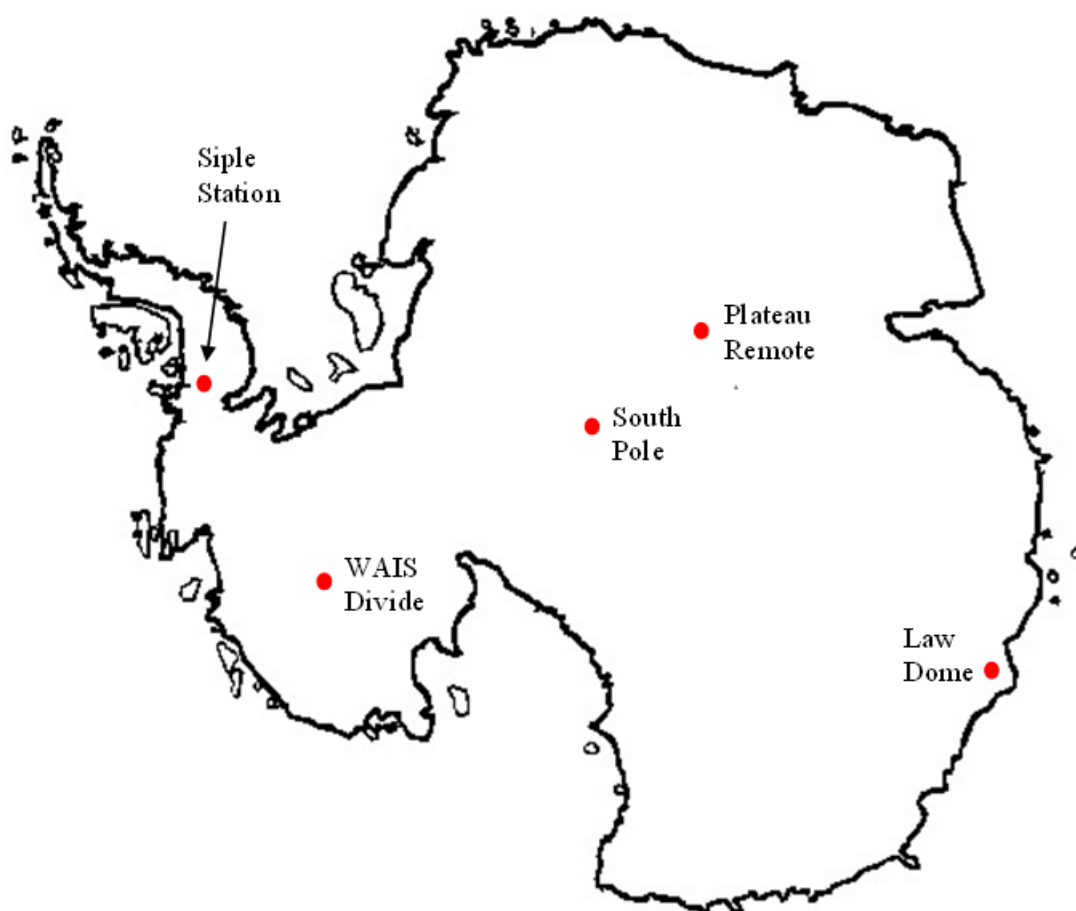
Volcanic flux can be used to represent the climate forcing of an event. Volcanic flux for the same event may be expected to vary at different ice core drilling sites for a number of reasons. This can be demonstrated through the volcanic eruption of Tambora that occurred in April of 1815. Located in Indonesia, Tambora is the largest and deadliest volcanic eruption in recorded history (Stothers, 1984). Due to the size of the eruption and Tambora's proximity to the equator, the sulfate signal from this event would be very prominent in ice cores from Antarctica. Table 1 does indicate an event occurred during this time period in SP19. Taking into consideration the SP19 uncertainty for this period (± 1 year), this event in SPC14 can be identified as Tambora.

Given when the eruption occurred and time for atmospheric transport, a large increase in sulfate would be expected during this time period. This is confirmed with a volcanic flux value of 5.16 kg km^{-2} for 1814. The subsequent year of 1815 had a volcanic flux of $35.33 \text{ kg} \cdot \text{km}^{-2}$ before decreasing to $13.94 \text{ kg} \cdot \text{km}^{-2}$ in 1816, for a total volcanic flux for Tambora being $54.43 \text{ kg} \cdot \text{km}^{-2}$.

Table 3 and Figure 19 show the Tambora volcanic flux values in ice cores from a number of locations in Antarctica (Cole-Dai *et al.*, 1997, Cole-Dai *et al.*, 2000, Cole-Dai *et al.*, 2021, Palmer *et al.*, 2002).

Table 3. Antarctica volcanic flux for Tambora.

Ice Core Location (Point in Figure 19)	Tambora Volcanic Flux ($\text{kg}\cdot\text{km}^{-2}$)	Reference
South Pole (SPC14)	54.4 (This work)	This work
Plateau Remote	22.4	(Cole-Dai <i>et al.</i> , 2000)
Siple Station	133.0	(Cole-Dai <i>et al.</i> , 1997)
WAIS Divide (WDC)	87.3	(Cole-Dai <i>et al.</i> , 2021)
Law Dome	79.8	(Palmer <i>et al.</i> , 2002)

**Figure 19.** Ice core locations in Antarctica where Tambora volcanic flux has been measured.

The Tambora event has a wide range of volcanic flux values: $22.4 \text{ kg}\cdot\text{km}^{-2}$ to $133.0 \text{ kg}\cdot\text{km}^{-2}$. This spatial variability may be attributed to variations in glaciological factors at ice core drilling sites. These factors include snow accumulation rate, temperature,

elevation, and winds potentially affecting transport of volcanic aerosols to ice core sites (Cole-Dai *et al.*, 1997, Palmer *et al.*, 2002). In addition, different techniques used to measure and quantify volcanic signals and calculate volcanic flux may also account for some of the variability (Palmer *et al.*, 2002).

These factors make comparisons of events via volcanic flux in different ice cores difficult. Comparisons of events in the same ice core is more feasible since sulfate deposition, and therefore volcanic flux, of events likely deposited at the ice core site in a consistent manner (Cole-Dai *et al.*, 1997). One way to compare events in different ice cores is to normalize volcanic flux by calculating the volcanic flux of all events relative to that of a well-established reference event present in all ice cores.

3.6 SPC14 Relative Flux

One value to use when comparing the same volcanic events in different ice cores is known as *relative flux*. Relative flux is defined as the ratio of the volcanic flux of the event of interest (f) to that of the reference event (f_{ref}). Tambora ($f_{Tambora}$) was chosen to be the reference event for this project, similarly to what was proposed in earlier studies (Cole-Dai *et al.*, 1997, Cole-Dai *et al.*, 2021). The advantage of using relative flux is that chemical species (in this case, sulfate) are assumed to be transported and deposited in each location in a similar manner for all events within the same ice core. This makes it easier to compare volcanic events in different ice cores to one another since it considers the glaciological conditions of the ice core drilling sites. For example, Event 20 in SPVR2022 identified at 1458 CE (± 2 years) can be compared with Event 26 in WHV2020 identified at 1459 CE using both volcanic flux and relative flux (Table 4) (Cole-Dai *et al.*, 2021).

Table 4. Comparison of volcanic flux and relative flux for the 1458/1459 event in two Antarctic volcanic records.

Record	Event Volcanic Flux (kg·km⁻²)	Tambora Volcanic Flux (kg·km⁻²)	Relative Flux
SPVR2022	58.72	54.43	1.08
WHV2020	94.91	87.26	1.09

Table 4 shows that the volcanic flux for this 1458/1459 volcanic event is very different in the ice core from the South Pole versus the one from WAIS Divide. The volcanic flux percent difference between the 1458 event in SPVR2022 and the 1459 event in WHV2020 is -38.1%. However, when using relative flux, the percent difference is only -0.9%. This demonstrates that relative flux is a better measure for comparing identical volcanic events in different ice cores. Relative flux was calculated for all 416 events in SPVR2022 (see Appendix A).

3.7 SPVR2022 Total Volcanic Flux and Events

SPVR2022 has a mean event volcanic flux of 11.31 kg·km⁻² with a mean event duration of 1.5 years. Total volcanic flux was calculated for each millennium and compared with the number of events to see if the average size of events in each millennium were similar (Figure 20).

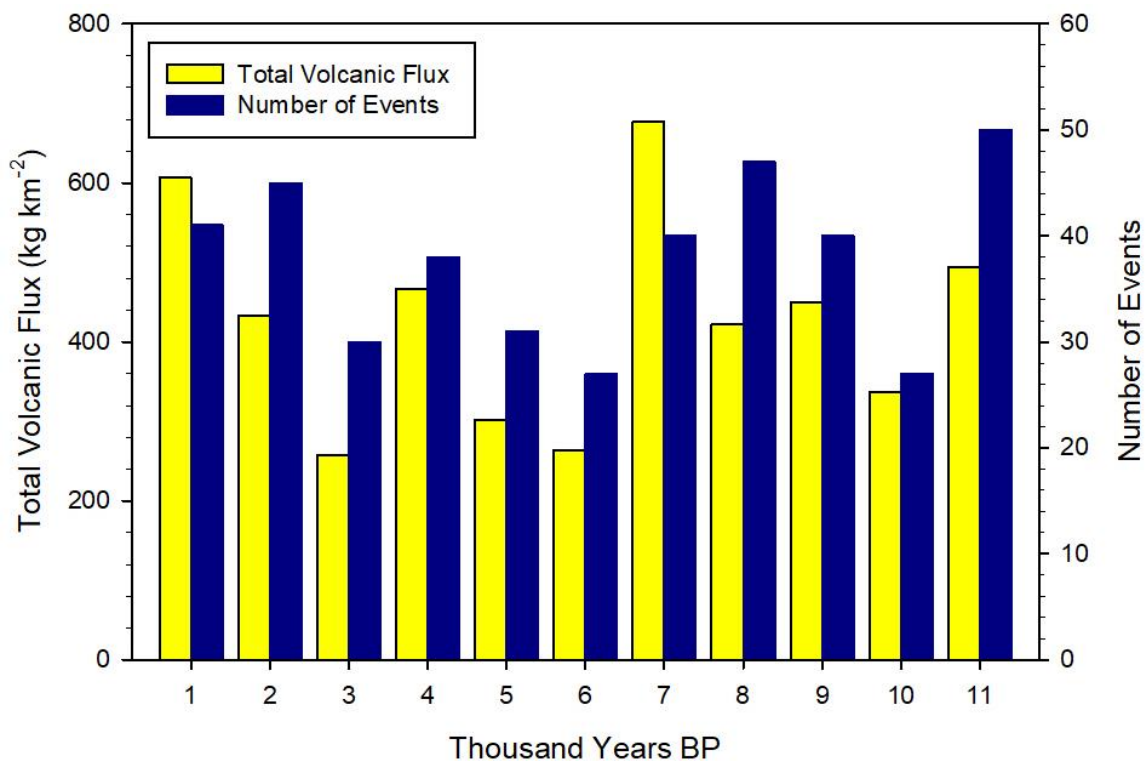


Figure 20. SPVR2022 total millennial volcanic flux and number of events comparison.

When the total millennial volcanic flux is compared with the number of events in each millennium, there does appear to be instances where a large number of events does not necessarily mean a large amount of volcanic flux. For example, the millennia with the largest number of events (eleventh millennium) does not have the largest amount of total volcanic flux. Both the first and seventh millennia BP have higher total volcanic flux values but lower number of events when compared to the eleventh millennium.

Table 5. SPVR2022 total millennial volcanic flux and number of events for every 1000 years BP.

Years BP	Total Volcanic Flux (kg·km ⁻²)	Number of Events
0 to 1000	606.95	41
1000 to 2000	433.45	45
2000 to 3000	257.00	30
3000 to 4000	466.10	38
4000 to 5000	301.47	31
5000 to 6000	264.06	27
6000 to 7000	676.38	40
7000 to 8000	422.26	47
8000 to 9000	449.24	40
9000 to 10K	336.44	27
10K to 11K	493.24	50

Table 5 shows the calculated values for total volcanic flux and number of events for each millennium. There appears to be less volcanic flux from 2000 to 6000 years BP with the highest amount being 466.10 kg·km⁻². The largest amounts of volcanic flux in SPVR2022 are seen in the most recent millennium (606.95 kg·km⁻²) and seventh millennium (676.38 kg·km⁻²).

4. DISCUSSION

4.1 Event Frequency During the Last 2000 years

The frequency of volcanic events in the last 2000 years has been studied in detail due to the availability of several volcanic records covering this time period. Volcanic records have been created from other ice cores drilled at Dome C and Plateau Remote, in addition to WAIS Divide, in Antarctica (Castellano *et al.*, 2004, Cole-Dai *et al.*, 2000, Cole-Dai *et al.*, 2021). These records allow for an in-depth comparison to those in SPVR2022 and discussion of the frequency of events, seen in Figure 21. This comparison may indicate that some records are better than others, helping to determine which records to use for comprehensive studies of volcanic impact on climate. In addition, differences among the records could reveal how volcanic sulfate is deposited and how signals are preserved in ice cores.

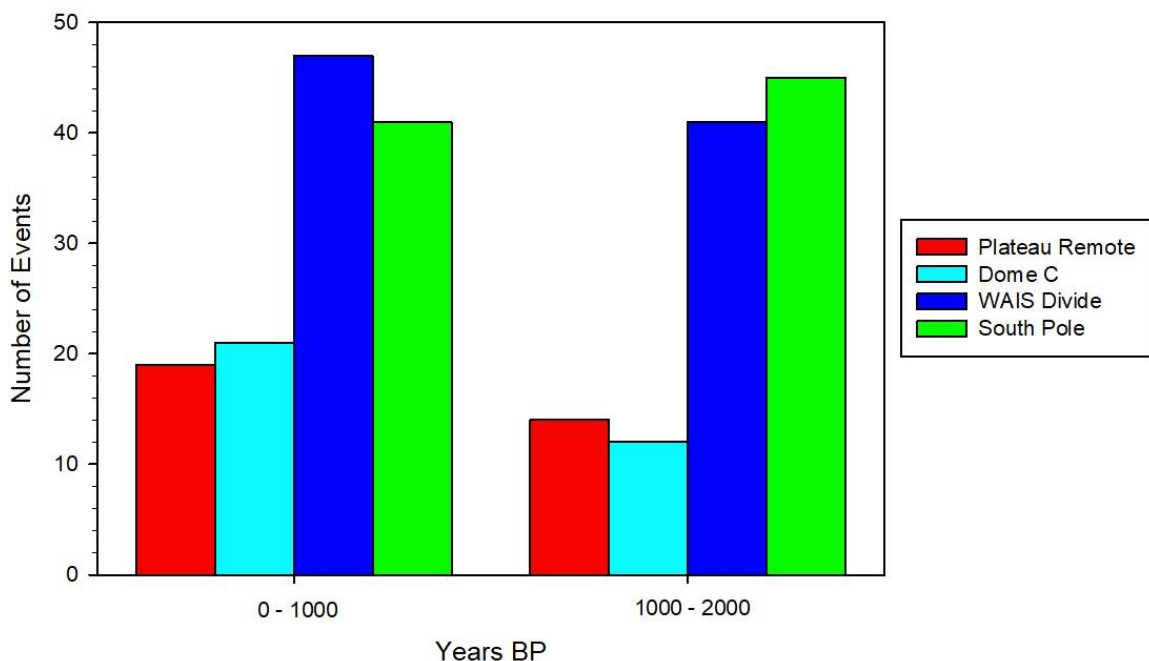


Figure 21. Number of events during the last 2000 years for different Antarctica ice core drilling sites.

Figure 21 shows two groups of records that are similar to each other: the two records from Plateau Remote and Dome C are one group, and the two more recent records (SPVR2022 and WHV2020) are the second group. During the first and second millennia CE, the number of events at Plateau Remote and Dome C are closer to 20 and 15, respectively. At WAIS Divide and South Pole, approximately 45 events are detected in the same time period.

The Dome C volcanic record was created using fast ion chromatography (FIC) which analyzed one sample per minute (Castellano *et al.*, 2004). The temporal resolution for Dome C was then calculated by multiplying this measurement rate by the melt rate which was between 4.0 and 7.0 cm min⁻¹ and then dividing by the accumulation rate in water equivalent (Castellano *et al.*, 2004). This sampling method creates a temporal resolution of approximately one sample per year throughout the Holocene due to the low accumulation rate at Dome C (approximately 4 cm snow per year) (Petit *et al.*, 1982). The volcanic record from Plateau Remote also had a sample resolution of approximately one sample per year due to the very low snow accumulation rate at this ice core drilling site (1.2 cm snow per year) (Cole-Dai *et al.*, 2000, Mosley-Thompson, 1996). Due to this accumulation rate, ALC was unable to be used to date the Plateau Remote ice core and dating was accomplished empirically instead (Cole-Dai *et al.*, 2000).

For the two more recent ice cores in Figure 21, WDC and SP14 had a much smaller sample size. WDC was dated using an ALC method relying on seasonal cycles of major ions, black carbon and trace elements at a sample size of approximately 1-2 cm (Sigl *et al.*, 2016). SPC14 was analyzed using capillary ion chromatography and allowed for samples to be collected at 1.1 cm on average for the Holocene (Winski *et al.*, 2019a). The much

higher snow accumulation rates at WAIS Divide and South Pole, along with the smaller sample sizes, resulted in a higher temporal resolution than in Plateau Remote and Dome C ice cores.

4.1.1 Detection Threshold Methodologies for Plateau Remote & Dome C

The volcanic record created at Plateau Remote relied on information from previous ice core studies that showed background sulfate concentrations in Antarctica remained relatively constant throughout the Holocene and that the background at Plateau Remote could be assumed constant as well (Cole-Dai *et al.*, 2000, Legrand, 1995). Because of this assumption, a mean of all points in the volcanic record was used to create the sulfate background. The mean plus two times the standard deviation was then applied to create the detection threshold (Cole-Dai *et al.*, 2000). In addition, another criterion for determining a volcanic event was that each event must have been above the threshold for two consecutive samples (Cole-Dai *et al.*, 2000).

The volcanic record from Dome C took a different approach. A log-normal approach used a 3% weighted fit smoothing procedure to create the background and two times the log of the standard deviation was added to create the detection threshold (Castellano *et al.*, 2004). Individual samples above the threshold were also subjectively evaluated to reject potential outliers (false positives) (Castellano *et al.*, 2004).

The different volcanic event detection methods along with the lower temporal resolution of the chemical analysis for Plateau Remote and Dome C ice cores can explain the differences when compared to the SPVR2022 and WHV2020 records. The low accumulation rates at Dome C (3 cm w.e. y^{-1} (The EPICA Dome C 2001-02 science and drilling teams, 2002)) and Plateau Remote (0.4 cm w.e. y^{-1} (Cole-Dai *et al.*, 2000)) do not

allow sub-annual resolution. This can cause some events that would be just above the detection threshold to be missed leading to a smaller number of detected events since sub-annual events cannot be seen.

The threshold method used for the volcanic record at Plateau Remote, while assuming a relatively constant background, does not account for small variations that are likely to occur. For example, if there is a period of time where many points lie below the mean baseline, the detection threshold may miss some events (example: Figure 13 in 3.1.1). Likewise, if there is a period of time where many points lie above the baseline, volcanic events may be assigned that are actually part of the natural baseline. While the volcanic record at Dome C did use a lognormal approach to consider natural background fluctuations, the low temporal resolution would cause some events to be missed by the threshold since potential sub-annual volcanic flux values would not be seen. Both detection methods used at Plateau Remote and Dome C do use two times the standard deviation or log of the standard deviation to establish a detection threshold.

4.1.2 Detection Threshold Methodologies for WHV2020 & SPVR2022

The advantage of the two recent volcanic records (WHV2020 and SPVR2022) is due to the improvements in sample collection and analysis. The smaller sample sizes in both of the recent volcanic records and higher accumulation rates at these locations allow for sub-annual sampling to occur. This process allows for more samples to be collected across a volcanic event creating high-resolution datasets. These high-resolution datasets give greater detail of seasonal variations of sulfate, showing a more variable baseline. To account for this variation, a running median was employed to determine the background level of natural sulfate, and then the threshold was created by using four times the median

absolute deviation (Cole-Dai *et al.*, 2021). The increase in resolution along with the similar approaches to volcanic detection may be used to explain why there are more events detected in WHV2020 and SPVR2022 than in the volcanic records from Plateau Remote and Dome C.

4.2 Holocene Event Frequency Comparison of SPV2022 to WHV2020

The high-resolution records from WDC and SPC14 allow for a detailed comparison of the frequency of events in the entire Holocene period. Figure 22 below shows how the number of events in WHV2020 and SPVR2022 compare to one another in each millennium of the Holocene.

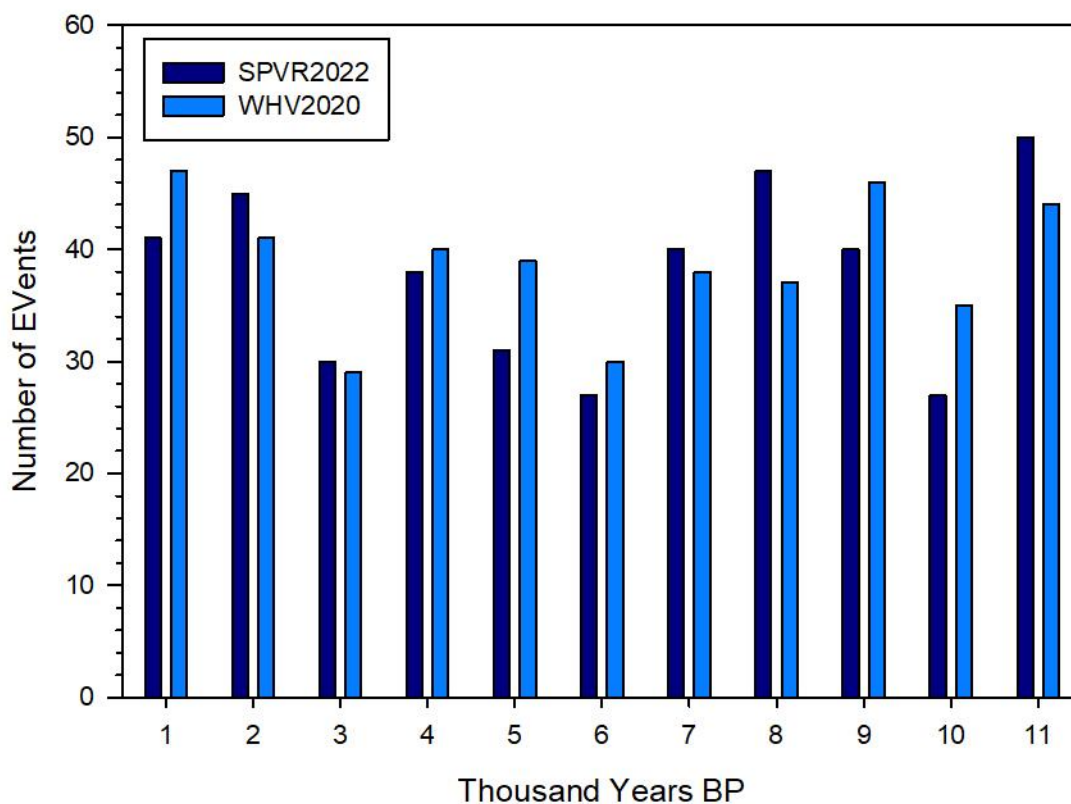


Figure 22. SPVR2022 & WHV2020 millennia event frequency comparison.

The millennia comparison between SPVR2022 and WHV2020 appears to show differences in the number of events between the two volcanic records. However,

uncertainties in the number of events must be considered as well. The mean number of events in SPVR2022 per millennium with uncertainty ($\pm 2\sigma$) is 38 ± 16 , and in WHV2020 it is 39 ± 12 . While there appears to be a higher event in WHV2020, uncertainties are large so that any difference between the two records may not be significant.

4.2.1 Eruption Frequency Statistical Comparison

The use of percent difference (Equation (7)) can give even greater insight between the volcanic events identified in SPVR2022 and WHV2020, shown in Table 6.

$$\text{percent difference} = \frac{\text{Events}_{\text{SPVR2022}} - \text{Events}_{\text{WHV2020}}}{\text{Events}_{\text{WHV2020}}} \times 100 \quad (7)$$

Table 6. Event frequency in SPVR2022 & WHV2020 for every 1000 years in the Holocene.

Years BP	# Events WHV2020	# Events SPVR2022	Difference	Percent Difference
0 to 1000 BP	47	41	6	-12.8%
1000 to 2000 BP	41	45	-4	9.8%
2000 to 3000 BP	29	30	-1	3.4%
3000 to 4000 BP	40	38	2	-5.0%
4000 to 5000 BP	39	31	8	-20.5%
5000 to 6000 BP	30	27	3	-10.0%
6000 to 7000 BP	38	40	-2	5.3%
7000 to 8000 BP	37	47	-10	27.0%
8000 to 9000 BP	46	40	6	-13.0%
9000 to 10K BP	35	27	8	-22.9%
10K to 11K BP	44	50	-6	13.6%
<i>Average per 1000 years</i>	<i>38.7</i>	<i>37.8</i>		
<i>Standard Deviation</i>	<i>5.9</i>	<i>8.0</i>		

The percent difference shows that from 1000 to 7000 years BP the number of events in each millennium is very similar with the exception of 4000 to 6000 BP. While the

percent differences may seem large at the beginning and end of the Holocene, one statistical test can be applied to see if the difference is statistically significant, and this can be accomplished by applying a paired t-test to the dataset in Table 6.

The paired t-test is ideal for this work as two sets of data from these ice cores are being compared for the number of events in each millennium. Thus, the null hypothesis for this work would be that no significant difference exists between the millennial numbers of the records, and the alternative hypothesis would be that the differences between the numbers are significant (non-zero). To test this hypothesis, the difference between each pair of millennia data points was first determined (Table 6). Next, the average of the difference, standard deviation of the difference, t-statistic, and p-value were calculated to complete the test. Table 7 shows the values for these statistical calculations.

Table 7. t-test statistical values.

Mean Difference	0.91
Std. Dev. Difference	6.01
t-statistic	0.50
p-value (n-1), two-tail	0.63

The value of most interest in Table 7 is the calculated p-value from the statistical test. This value is calculated using the t-statistic and a t-table. A p-value of 0.05 or less usually indicates the hypothesis should be rejected at the 95% confidence level. Since the calculated p-value in Table 7 is greater than 0.05, the null hypothesis (no difference between the records) cannot be rejected, meaning that either WHV2020 or SPVR2022 can be used to determine the number of events in each millennium of the Holocene. This suggests that SPVR2022 corroborates the millennial event frequency found in the

WHV2020 record. Additionally, two different sites with different glaciological conditions (snow accumulation rate, elevation, proximity to the coast or interior of Antarctica) can be used to determine the frequency of events during the Holocene.

4.3 Ten Largest Volcanic Events in SPVR2022 & WHV2020

The ten largest events by relative flux not including Tambora in WHV2020 are not the same as those in SPVR2022; however, some events appear in both lists (Cole-Dai *et al.*, 2021). Table 8 and Table 9 contain the data for both SPVR2022 and WHV2020, respectively. Highlighted rows in each table indicate the same event in both records.

Table 8. Ten largest events by relative flux in SPVR2022.

Rank	Event Number	Year BP	Year CE	Total Volcanic Flux kg·km ⁻²	Relative Flux	Duration Year
1	260	7177	-5227	110.58	2.03	2
2	183	4860	-2910	104.21	1.91	3
3	221	6328	-4378	100.37	1.84	4
4	230	6482	-4532	93.05	1.71	3
5	234	6554	-4604	88.59	1.63	4
6	121	3124	-1174	79.6	1.46	4
7	360	9790	-7840	78.38	1.44	3
8	280	7572	-5622	76.27	1.40	4
9	27	692	1258	71.51	1.31	2
10	370	10082	-8132	68.12	1.25	4

Table 9. Ten largest events by relative flux in WHV2020.

Rank	Event Number	Year BP	Year CE	Total Volcanic Flux kg km ⁻²	Relative Flux	Duration Year
1	425	10957	-9008	182.12	2.09	3
2	272	7177	-5228	160.86	1.84	3
3	288	7572	-5623	153.68	1.76	3
4	193	4860	-2911	110.75	1.27	2
5	389	10115	-8166	108.19	1.24	5
6	388	10080	-8131	105.66	1.21	2
7	26	491	1459	94.91	1.09	3
8	99	2376	-427	92.33	1.06	3
9	399	10356	-8407	90.99	1.04	3
10	292	7793	-5844	88.30	1.01	3

The largest event in SPVR2022 by total volcanic flux is Event 260 (7177 years BP) with a value of 110.58 kg·km⁻². The WHV2020 largest event is Event 425 (10,957 years BP) with a value of 182.12 kg·km⁻², about 80% larger than the largest event in SPVR2022. Four of the largest events are found in both SPVR2022 and WHV2020, albeit ranked differently in each record. For example, the largest event in SPVR2022 (Event 260) is the second largest in WHV2020.

While some events appear in both top ten lists, there are important differences. Because both SPVR2022 and WHV2020 are volcanic records covering the entire Holocene, a discussion can occur on why differences exist between the records and potential implications of these differences. Understanding these differences can help to advance the current understanding of sulfate atmospheric transport and to allow detailed study of the volcano-climate connection.

4.3.1 Differences in the Largest Events in SPVR2022 & WHV2020

One of the main differences between the two records would be the amount of volcanic flux in the largest events. The largest event identified in WHV2020 (Event 425, $182.12 \text{ kg}\cdot\text{km}^{-2}$) is approximately 80% more in size in total volcanic flux than the largest event in SPVR2022 (Event 260, $110.58 \text{ kg}\cdot\text{km}^{-2}$). While not an identical event comparison since SPVR2022's largest event occurred 7177 years BP and WHV2020's took place 10,957 years BP, the amount of volcanic flux deposited at each location can give further insight into sulfate deposition in Antarctica. Relative flux is a better comparison tool for identical events in other ice cores, but the differences in volcanic flux can help to understand how glaciological conditions vary across Antarctica.

For example, the locations of both ice core drilling sites may explain the difference in the amounts of sulfate deposition. WAIS Divide is closer to the coast and at a lower elevation than South Pole. The distance between the ice core site and the erupting volcano may influence the amount of sulfate deposited at the site. More sulfate may potentially be deposited at WAIS Divide than at South Pole due to shorter distance for sulfate aerosol transport if the erupting volcano is located offshore, as more volcanic aerosols are removed from the atmosphere during longer transport. The distance between the ice core site and the erupting volcano may influence the amount of sulfate deposited at the site. In addition, since WAIS Divide is at a lower elevation than the South Pole, less sulfate from tropospheric volcanic eruptions is likely to deposit at South Pole.

While the total volcanic flux between the largest events can help to identify causes of the differences, relative flux can allow for a more detailed discussion on sulfate atmospheric transport and glaciological environments at each ice core drilling site. For

instance, the volcanic event at 7177 years BP in both SPVR2022 and WHV2020 has relative flux values of 2.03 and 1.84, respectively. This is only a 10.3% difference indicating that this event had enough volcanic flux to be deposited in a similar manner at both locations. This could be attributed to a stratospheric eruption which is likely due to this event being one of the largest in both records. However, a volcanic event that also occurred in both records 4860 years BP has a relative flux value of 1.91 in SPVR2022 and 1.27 in WHV2020, a 50.4% difference. This difference indicates that more of the volcanic sulfate in flux from this event deposited at the South Pole than at WAIS Divide. Since the relative flux considers glaciological conditions and attempts to mitigate these factors, one speculative possibility for the difference between the two sites may be attributed to the difference in proximity of the erupting volcano to the drill sites.

Another (more plausible) possibility for the relative flux difference would be the polar vortex. The polar vortex is a form of atmospheric circulation which can occur in both the troposphere and stratosphere with west-to-east air flows encircling the poles (Vaugh *et al.*, 2017). The polar vortex occurs each winter and is a consequence of the large-scale temperature gradients that exist between the mid-latitudes and the pole, being stronger in the winter when there is no solar radiation and being weaker in the summer when solar radiation returns (Vaugh *et al.*, 2017). Polar vortexes can bring much cooler stratosphere down to the surface at the poles and enhance the volcanic sulfate flux if an eruption injects SO₂ directly into the stratosphere.

4.4 Volcanic Events and the Santorini (Thera) Eruption in 17th Century BCE

The Santorini eruption, also known as Thera, is known to be a large Mediterranean eruption that occurred in the 17th century BCE and is a crucial tie point in many different

chronologies such as radiocarbon dating, tree rings, and Greenland ice cores (Hammer, 1977, Manning; *et al.*, 2006, Salzer and Hughes, 2017). The Thera eruption could be useful in synchronizing all the different types of chronologies with one another. However, this event is subject to considerable debate as to the exact time the eruption occurred. Determining when this eruption occurred is important to the synchronization of Aegean, Egyptian, and Near Eastern civilization chronologies (McAneney and Baillie, 2019).

Much of the debate is centered around the uncertainties of the ages of events which are inherent to any technique to determine chronology (Cole-Dai *et al.*, 2021). Recent re-evaluation of tree ring chronologies and the Greenland Ice Core Chronology of 2005 (GICC05), however, has suggested the Thera eruption to have occurred between 1600-1700 BCE, specifically the years 1653, 1627, and 1610 BCE in the GICC05 timescale (McAneney and Baillie, 2019). While McAneney and Baillie suggest this time period for the Thera eruption, they also do not believe any of the volcanic events in the Greenland ice core records to be Thera. Their reasoning is based on the fact that two of the volcanic signals (1653 and 1610 BCE events) are near the outer boundaries of radiocarbon-dated Thera artifacts, and tephra from a different volcano (Aniakchak in Alaska) matched the tephra found in the ice cores for the 1627 BCE event (Coulter *et al.*, 2012). The new SPVR2022 record can contribute to the Thera discussion via the high-temporal resolution of the volcanic record.

SPVR2022 does have events identified at the years suggested by McAneney and Baillie, specifically 1655, 1628, and 1610 BCE. In addition, the WHV2020 record also has the volcanic events at the same time periods. Table 10 below shows the comparison between SPVR2022 and WHV2020 for these years.

Table 10. Potential Thera comparison in SPVR2022 & WHV2020.

	Year (BCE)	Duration	Total Volcanic Flux (kg·km ⁻²)	Relative Flux
WHV2020	1657	4	40.0	0.46
	1629	2	18.2	0.21
	1612	3	17.0	0.19
SPVR2022	1655	3	29.4	0.54
	1628	1	15.8	0.29
	1612	1	5.9	0.11

The relative flux for the 17th century BCE events is very similar to one another, indicating that a similar amount of sulfate was deposited at both ice core sites. This implies that the event(s) contributing to these three years likely had sulfate aerosols transported in a similar manner.

Since these events are detected in SPVR2022, WHV2020, and the Greenland ice cores, these records indicate that the aerosols of these eruptions were distributed globally. Volcanic events detected in ice cores are influenced by the location of the erupting volcano, and aerosols from equatorial eruptions can be transported to both Antarctica and Greenland (Palmer *et al.*, 2002). These records thus indicate that the eruption location was most likely close to the equator. However, Thera is located 36.4°N which would preclude the eruption from being detected in any Antarctic ice core volcanic record as it is too far north of the equator.

The possibility exists that the Thera eruption did occur simultaneously with a southern hemisphere volcanic eruption. However, large differences in the relative flux values between the Antarctic and Greenland volcanic records would be expected if they were indeed different eruptions, but the relative flux values for all three records are similar

in magnitude (Greenland volcanic records relative flux values: 0.27 for the 1629 event and 0.17 for the 1612 event, compared to the values in SPVR2022 and WHV2020 in Table 10) (Cole-Dai *et al.*, 2021, Zielinski; *et al.*, 1994).

5. CONCLUSIONS

The South Pole Ice Core (SPC14) and the corresponding ice core SPC14 data has been used to create a new volcanic record covering the Holocene, a period of time spanning the most recent 11,000 years and the first of its kind from a South Pole ice core. This new volcanic record, SPVR2022, identifies 416 events that occurred during the Holocene with no apparent trend in the frequency of events between millennia. Further analysis indicates when a similar methodology is used to discriminate volcanic events from a natural sulfate background (such as in WHV2020), no statistical difference exists between the millennial frequency of events in these two records.

Comparisons were made to WHV2020, the only other high-resolution volcanic record covering the same time period from Antarctica. The total volcanic flux for the largest events in each record show higher values at WAIS Divide than at the South Pole. These differences may be attributed to sulfate atmospheric transport, whether the aerosol cloud of the eruption was limited to the troposphere or reached the stratosphere, and elevation differences between the two sites. In addition, relative flux differences exist between identical events in both records, indicating that volcanic sulfate deposited more at one location over the other. These differences may be due to volcano proximity to each site or atmospheric transport mechanisms such as the polar vortex.

The potential of the Santorini eruption, also known as Thera, was examined in SPVR2022 and the examination validates the relative flux values found in the WHV2020 and GICC05 records. SPVR2022 provides more evidence that the three eruptions detected in the 17th century BCE should not be attributed to Thera. Since Thera is located in the mid latitudes of the Northern Hemisphere and the volcanic signature of the three events in

the 17th century BCE are seen in both Greenland and Antarctica ice cores, this indicates equatorial, or low latitude, eruptions are most likely the source of these volcanic signatures.

APPENDIX A – SPVR2022

Event Number	Year BP	Year CE	Total Volcanic Flux kg km ⁻²	Relative Flux	Duration Year
1	-20	1970	3.34	0.06	1
2	-15	1965	4.17	0.08	1
3	-13	1963	10.94	0.20	1
4	64	1886	3.34	0.06	1
5	67	1883	16.41	0.30	2
6	87	1863	6.12	0.11	1
7	93	1857	2.92	0.05	1
8	112	1838	7.93	0.15	2
9	136	1814	54.43	1.00	3
10	141	1809	31.02	0.57	3
11	169	1781	3.73	0.07	1
12	255	1695	22.60	0.42	3
13	308	1642	5.54	0.10	1
14	328	1622	6.68	0.12	1
15	350	1600	20.18	0.37	3
16	356	1594	25.75	0.47	4
17	395	1555	4.11	0.08	1
18	443	1507	5.62	0.10	1
19	473	1477	4.25	0.08	1
20	492	1458	58.72	1.08	4
21	563	1387	3.26	0.06	1
22	606	1344	17.32	0.32	3
23	648	1302	4.26	0.08	1
24	664	1286	24.07	0.44	2
25	674	1276	38.53	0.71	2
26	682	1268	16.09	0.30	2
27	692	1258	71.51	1.31	2
28	712	1238	5.09	0.09	1
29	720	1230	30.75	0.56	2
30	756	1194	4.01	0.07	1
31	760	1190	3.99	0.07	1
32	771	1179	3.75	0.07	1
33	780	1170	23.00	0.42	3
34	823	1127	4.50	0.08	1
35	840	1110	16.39	0.30	3
36	880	1070	6.45	0.12	2
37	906	1044	12.35	0.23	3
38	915	1035	4.98	0.09	1

39	926	1024	3.38	0.06	1
40	936	1014	3.34	0.06	1
41	986	964	12.13	0.22	2
42	1001	949	4.21	0.08	1
43	1023	927	4.43	0.08	1
44	1027	923	3.28	0.06	1
45	1047	903	9.91	0.18	1
46	1061	889	3.17	0.06	1
47	1087	863	5.25	0.10	1
48	1093	857	4.67	0.09	1
49	1095	855	3.89	0.07	1
50	1112	838	3.93	0.07	1
51	1129	821	5.51	0.10	1
52	1199	751	5.73	0.11	1
53	1267	683	46.70	0.86	5
54	1309	641	4.25	0.08	1
55	1321	629	4.38	0.08	1
56	1352	598	4.45	0.08	1
57	1357	593	3.68	0.07	1
58	1359	591	3.51	0.06	1
59	1375	575	29.54	0.54	3
60	1410	540	17.48	0.32	2
61	1413	537	3.31	0.06	1
62	1422	528	3.50	0.06	1
63	1488	462	4.94	0.09	1
64	1516	434	32.19	0.59	2
65	1592	358	10.46	0.19	2
66	1598	352	9.82	0.18	1
67	1624	326	3.29	0.06	1
68	1647	303	17.91	0.33	2
69	1683	267	9.34	0.17	2
70	1713	237	19.02	0.35	2
71	1745	205	23.87	0.44	2
72	1781	169	25.76	0.47	2
73	1794	156	3.68	0.07	1
74	1800	150	4.26	0.08	1
75	1806	144	4.32	0.08	1
76	1825	125	10.73	0.20	2
77	1827	123	7.69	0.14	1
78	1844	106	3.27	0.06	1
79	1851	99	6.39	0.12	1
80	1875	75	3.18	0.06	1
81	1892	58	3.55	0.07	1

82	1918	32	6.29	0.12	1
83	1937	13	3.67	0.07	1
84	1961	-11	19.13	0.35	3
85	1972	-22	14.19	0.26	2
86	1999	-49	11.72	0.22	2
87	2036	-86	3.53	0.06	1
88	2057	-107	4.91	0.09	1
89	2061	-111	4.76	0.09	1
90	2086	-136	9.39	0.17	1
91	2103	-153	4.56	0.08	1
92	2107	-157	4.69	0.09	1
93	2109	-159	4.01	0.07	1
94	2130	-180	3.43	0.06	1
95	2132	-182	5.13	0.09	1
96	2175	-225	11.56	0.21	2
97	2212	-262	32.21	0.59	4
98	2292	-342	5.72	0.11	1
99	2306	-356	10.44	0.19	1
100	2309	-359	4.65	0.09	1
101	2344	-394	3.32	0.06	1
102	2348	-398	16.12	0.30	2
103	2376	-426	49.94	0.92	3
104	2433	-483	3.42	0.06	1
105	2526	-576	16.46	0.30	3
106	2532	-582	4.98	0.09	1
107	2549	-599	4.42	0.08	1
108	2629	-679	4.14	0.08	1
109	2644	-694	5.56	0.10	1
110	2668	-718	7.78	0.14	1
111	2681	-731	3.53	0.06	1
112	2718	-768	3.46	0.06	1
113	2781	-831	7.89	0.14	2
114	2834	-884	4.07	0.07	1
115	2898	-948	5.11	0.09	1
116	2922	-972	7.81	0.14	2
117	3035	-1085	6.83	0.13	2
118	3037	-1087	3.21	0.06	1
119	3093	-1143	3.19	0.06	1
120	3102	-1152	4.43	0.08	1
121	3124	-1174	79.60	1.46	4
122	3134	-1184	3.76	0.07	1
123	3167	-1217	3.18	0.06	1
124	3206	-1256	7.52	0.14	1

125	3256	-1306	3.23	0.06	1
126	3275	-1325	10.23	0.19	2
127	3300	-1350	3.52	0.06	1
128	3312	-1362	33.31	0.61	3
129	3322	-1372	3.80	0.07	1
130	3347	-1397	3.49	0.06	1
131	3358	-1408	18.96	0.35	3
132	3367	-1417	12.26	0.23	3
133	3388	-1438	3.20	0.06	1
134	3479	-1529	9.02	0.17	1
135	3482	-1532	3.71	0.07	1
136	3500	-1550	27.06	0.50	3
137	3507	-1557	3.90	0.07	1
138	3521	-1571	4.05	0.07	1
139	3529	-1579	3.17	0.06	1
140	3560	-1610	3.49	0.06	1
141	3562	-1612	5.93	0.11	1
142	3578	-1628	15.83	0.29	1
143	3605	-1655	29.39	0.54	3
144	3640	-1690	3.67	0.07	1
145	3668	-1718	4.66	0.09	1
146	3673	-1723	3.18	0.06	1
147	3675	-1725	3.30	0.06	1
148	3816	-1866	3.66	0.07	1
149	3818	-1868	3.97	0.07	1
150	3831	-1881	41.53	0.76	5
151	3836	-1886	4.92	0.09	1
152	3875	-1925	35.65	0.65	3
153	3925	-1975	20.59	0.38	4
154	3990	-2040	31.70	0.58	2
155	4048	-2098	3.11	0.06	1
156	4090	-2140	3.57	0.07	1
157	4118	-2168	3.36	0.06	1
158	4142	-2192	3.73	0.07	1
159	4158	-2208	4.14	0.08	1
160	4178	-2228	3.97	0.07	1
161	4216	-2266	4.44	0.08	1
162	4223	-2273	19.61	0.36	3
163	4231	-2281	6.19	0.11	1
164	4249	-2299	3.18	0.06	1
165	4278	-2328	8.59	0.16	2
166	4306	-2356	7.33	0.13	1
167	4352	-2402	4.37	0.08	1

168	4354	-2404	3.33	0.06	1
169	4410	-2460	19.75	0.36	3
170	4421	-2471	10.40	0.19	1
171	4440	-2490	4.94	0.09	1
172	4444	-2494	3.50	0.06	1
173	4498	-2548	3.93	0.07	1
174	4521	-2571	4.10	0.08	1
175	4524	-2574	14.24	0.26	2
176	4627	-2677	3.23	0.06	1
177	4634	-2684	12.69	0.23	3
178	4644	-2694	7.72	0.14	1
179	4647	-2697	4.17	0.08	1
180	4667	-2717	14.92	0.27	2
181	4790	-2840	3.19	0.06	1
182	4795	-2845	3.03	0.06	1
183	4860	-2910	104.21	1.91	3
184	4941	-2991	2.98	0.05	1
185	4966	-3016	5.55	0.10	1
186	5052	-3102	19.92	0.37	3
187	5058	-3108	3.41	0.06	1
188	5070	-3120	12.26	0.23	2
189	5101	-3151	8.46	0.16	2
190	5108	-3158	3.25	0.06	1
191	5110	-3160	4.20	0.08	1
192	5232	-3282	14.37	0.26	2
193	5244	-3294	12.08	0.22	2
194	5317	-3367	19.40	0.36	4
195	5357	-3407	5.22	0.10	1
196	5405	-3455	3.44	0.06	1
197	5447	-3497	4.22	0.08	1
198	5451	-3501	7.58	0.14	2
199	5468	-3518	29.16	0.54	2
200	5561	-3611	8.57	0.16	2
201	5613	-3663	4.30	0.08	1
202	5618	-3668	17.40	0.32	2
203	5651	-3701	5.90	0.11	1
204	5666	-3716	8.81	0.16	2
205	5676	-3726	11.38	0.21	2
206	5732	-3782	3.09	0.06	1
207	5844	-3894	3.20	0.06	1
208	5887	-3937	10.36	0.19	1
209	5899	-3949	4.27	0.08	1
210	5920	-3970	13.88	0.26	2

211	5977	-4027	17.65	0.32	3
212	5983	-4033	8.28	0.15	2
213	6038	-4088	3.38	0.06	1
214	6129	-4179	4.59	0.08	1
215	6166	-4216	12.79	0.23	2
216	6223	-4273	3.36	0.06	1
217	6268	-4318	10.46	0.19	1
218	6284	-4334	61.40	1.13	6
219	6307	-4357	9.90	0.18	2
220	6312	-4362	18.84	0.35	3
221	6328	-4378	100.37	1.84	4
222	6336	-4386	3.79	0.07	1
223	6347	-4397	13.09	0.24	1
224	6360	-4410	23.05	0.42	3
225	6384	-4434	5.90	0.11	1
226	6440	-4490	4.07	0.07	1
227	6442	-4492	7.33	0.13	1
228	6450	-4500	14.28	0.26	2
229	6457	-4507	3.70	0.07	1
230	6482	-4532	93.05	1.71	3
231	6522	-4572	7.69	0.14	2
232	6539	-4589	3.54	0.07	1
233	6545	-4595	23.22	0.43	2
234	6554	-4604	88.59	1.63	4
235	6578	-4628	8.16	0.15	2
236	6606	-4656	3.49	0.06	1
237	6614	-4664	12.02	0.22	2
238	6639	-4689	10.83	0.20	1
239	6648	-4698	6.01	0.11	1
240	6654	-4704	35.01	0.64	2
241	6662	-4712	33.96	0.62	2
242	6688	-4738	3.55	0.07	1
243	6695	-4745	6.17	0.11	1
244	6708	-4758	3.91	0.07	1
245	6723	-4773	5.98	0.11	1
246	6745	-4795	5.08	0.09	1
247	6776	-4826	4.60	0.08	1
248	6822	-4872	3.02	0.06	1
249	6881	-4931	4.95	0.09	1
250	6888	-4938	5.66	0.10	1
251	6924	-4974	3.90	0.07	1
252	6954	-5004	3.69	0.07	1
253	7022	-5072	6.20	0.11	1

254	7041	-5091	3.07	0.06	1
255	7048	-5098	3.44	0.06	1
256	7142	-5192	7.63	0.14	1
257	7149	-5199	3.27	0.06	1
258	7157	-5207	3.14	0.06	1
259	7173	-5223	3.94	0.07	1
260	7177	-5227	110.58	2.03	2
261	7185	-5235	3.26	0.06	1
262	7238	-5288	4.39	0.08	1
263	7241	-5291	7.18	0.13	1
264	7252	-5302	6.23	0.11	1
265	7255	-5305	3.79	0.07	1
266	7262	-5312	3.55	0.07	1
267	7276	-5326	3.45	0.06	1
268	7304	-5354	4.60	0.08	1
269	7332	-5382	4.87	0.09	1
270	7370	-5420	3.95	0.07	1
271	7385	-5435	3.97	0.07	1
272	7405	-5455	3.66	0.07	1
273	7407	-5457	4.42	0.08	1
274	7430	-5480	5.03	0.09	1
275	7458	-5508	8.81	0.16	2
276	7464	-5514	11.12	0.20	2
277	7515	-5565	3.67	0.07	1
278	7528	-5578	3.35	0.06	1
279	7560	-5610	11.53	0.21	2
280	7572	-5622	76.27	1.40	4
281	7578	-5628	4.95	0.09	1
282	7584	-5634	4.71	0.09	1
283	7618	-5668	3.68	0.07	1
284	7662	-5712	3.58	0.07	1
285	7674	-5724	4.15	0.08	1
286	7686	-5736	3.29	0.06	1
287	7698	-5748	3.22	0.06	1
288	7701	-5751	3.86	0.07	1
289	7770	-5820	3.57	0.07	1
290	7793	-5843	8.93	0.16	1
291	7833	-5883	3.53	0.06	1
292	7835	-5885	3.87	0.07	1
293	7859	-5909	15.93	0.29	3
294	7871	-5921	14.23	0.26	2
295	7889	-5939	4.94	0.09	1
296	7933	-5983	4.66	0.09	1

297	7972	-6022	5.83	0.11	1
298	7976	-6026	3.75	0.07	1
299	7993	-6043	3.21	0.06	1
300	8027	-6077	3.36	0.06	1
301	8065	-6115	3.26	0.06	1
302	8093	-6143	14.94	0.27	3
303	8147	-6197	4.16	0.08	1
304	8174	-6224	4.08	0.07	1
305	8178	-6228	29.66	0.54	3
306	8229	-6279	65.79	1.21	4
307	8252	-6302	18.65	0.34	1
308	8269	-6319	11.93	0.22	1
309	8288	-6338	10.04	0.18	2
310	8321	-6371	6.65	0.12	2
311	8364	-6414	26.15	0.48	2
312	8387	-6437	3.56	0.07	1
313	8405	-6455	16.10	0.30	3
314	8411	-6461	14.29	0.26	2
315	8443	-6493	17.74	0.33	2
316	8449	-6499	8.38	0.15	2
317	8451	-6501	3.77	0.07	1
318	8456	-6506	3.79	0.07	1
319	8462	-6512	3.57	0.07	1
320	8493	-6543	3.98	0.07	1
321	8505	-6555	5.33	0.10	1
322	8510	-6560	3.21	0.06	1
323	8534	-6584	10.03	0.18	1
324	8552	-6602	6.29	0.12	1
325	8554	-6604	3.71	0.07	1
326	8605	-6655	10.14	0.19	1
327	8614	-6664	52.46	0.96	3
328	8679	-6729	3.22	0.06	1
329	8750	-6800	4.18	0.08	1
330	8783	-6833	8.86	0.16	1
331	8849	-6899	5.10	0.09	1
332	8854	-6904	6.55	0.12	1
333	8863	-6913	5.48	0.10	1
334	8880	-6930	9.98	0.18	2
335	8886	-6936	4.55	0.08	1
336	8934	-6984	3.68	0.07	1
337	8943	-6993	19.14	0.35	3
338	8988	-7038	9.54	0.18	1
339	8995	-7045	3.94	0.07	1

340	9009	-7059	3.51	0.06	1
341	9032	-7082	3.74	0.07	1
342	9065	-7115	44.09	0.81	3
343	9080	-7130	3.33	0.06	1
344	9086	-7136	6.57	0.12	1
345	9117	-7167	3.86	0.07	1
346	9135	-7185	3.83	0.07	1
347	9153	-7203	7.43	0.14	1
348	9185	-7235	3.50	0.06	1
349	9194	-7244	6.77	0.12	2
350	9312	-7362	8.79	0.16	2
351	9352	-7402	30.61	0.56	4
352	9366	-7416	3.66	0.07	1
353	9413	-7463	4.68	0.09	1
354	9426	-7476	3.42	0.06	1
355	9447	-7497	15.48	0.28	2
356	9541	-7591	6.19	0.11	2
357	9603	-7653	8.19	0.15	2
358	9682	-7732	23.34	0.43	2
359	9726	-7776	14.31	0.26	2
360	9790	-7840	78.38	1.44	3
361	9811	-7861	3.58	0.07	1
362	9837	-7887	25.45	0.47	4
363	9879	-7929	3.23	0.06	1
364	9933	-7983	5.72	0.11	1
365	9973	-8023	5.50	0.10	1
366	9985	-8035	9.28	0.17	2
367	10011	-8061	3.89	0.07	1
368	10020	-8070	10.68	0.20	1
369	10047	-8097	8.61	0.16	2
370	10082	-8132	68.12	1.25	4
371	10102	-8152	4.95	0.09	1
372	10108	-8158	7.17	0.13	1
373	10116	-8166	4.80	0.09	1
374	10141	-8191	3.30	0.06	1
375	10211	-8261	3.31	0.06	1
376	10224	-8274	7.98	0.15	1
377	10234	-8284	9.15	0.17	1
378	10236	-8286	10.25	0.19	1
379	10259	-8309	4.36	0.08	1
380	10323	-8373	4.31	0.08	1
381	10325	-8375	5.28	0.10	1
382	10344	-8394	4.88	0.09	1

383	10357	-8407	44.25	0.81	3
384	10360	-8410	3.34	0.06	1
385	10388	-8438	12.52	0.23	2
386	10397	-8447	3.62	0.07	1
387	10399	-8449	3.64	0.07	1
388	10402	-8452	15.93	0.29	2
389	10432	-8482	12.92	0.24	2
390	10435	-8485	3.60	0.07	1
391	10463	-8513	4.02	0.07	1
392	10475	-8525	27.27	0.50	5
393	10478	-8528	9.18	0.17	1
394	10497	-8547	17.22	0.32	2
395	10527	-8577	4.85	0.09	1
396	10570	-8620	6.65	0.12	1
397	10589	-8639	4.77	0.09	1
398	10598	-8648	8.10	0.15	1
399	10632	-8682	10.17	0.19	2
400	10634	-8684	5.71	0.10	1
401	10698	8748	3.12	0.06	1
402	10709	-8759	3.96	0.07	1
403	10721	-8771	4.49	0.08	1
404	10724	-8774	4.65	0.09	1
405	10729	-8779	3.79	0.07	1
406	10731	-8781	3.63	0.07	1
407	10733	-8783	4.16	0.08	1
408	10788	-8838	5.56	0.10	1
409	10790	-8840	3.72	0.07	1
410	10862	-8912	4.80	0.09	1
411	10874	-8924	3.59	0.07	1
412	10906	-8956	5.04	0.09	1
413	10937	-8987	5.41	0.10	1
414	10958	-9008	60.05	1.10	4
415	10970	-9020	4.44	0.08	1
416	10982	-9032	14.03	0.26	2

REFERENCES

- About SPICEcore. <https://spicecore.org/about/#overview> (accessed February 8, 2022).
- Banta, J. R. *et al.*, **2008**, Spatial and temporal variability in snow accumulation at the West Antarctic Ice Sheet Divide over recent centuries. *Journal of Geophysical Research* 113 (D23).
- Breton, D. J. *et al.*, **2012**, Quantifying signal dispersion in a hybrid ice core melting system. *Environ Sci Technol* 46 (21), 11922-8.
- Castellano, E. *et al.*, **2004**, Volcanic eruption frequency over the last 45 ky as recorded in Epica-Dome C ice core (East Antarctica) and its relationship with climatic changes. *Global and Planetary Change* 42 (1-4), 195-205.
- Cole-Dai, J. *et al.*, **2006**, High Speed, High Resolution, and Continuous Chemical Analysis of Ice Cores Using a Melter and Ion Chromatography. *Environ Sci Technol* 40, 6764-6769.
- Cole-Dai, J. *et al.*, **1997**, Annually resolved southern hemisphere volcanic history from two Antarctic ice cores. *Journal of Geophysical Research: Atmospheres* 102 (D14), 16761-16771.
- Cole-Dai, J. *et al.*, **2000**, A 4100-year record of explosive volcanism from an East Antarctica ice core. *Journal of Geophysical Research: Atmospheres* 105 (D19), 24431-24441.
- Cole-Dai, J., **2010**, Volcanoes and climate. *WIREs Climate Change* 1 (6), 824-839.
- Cole-Dai, J. *et al.*, **2021**, Comprehensive Record of Volcanic Eruptions in the Holocene (11,000 years) From the WAIS Divide, Antarctica Ice Core. *Journal of Geophysical Research: Atmospheres* 126 (7).
- Coulter, S. E. *et al.*, **2012**, Holocene tephras highlight complexity of volcanic signals in Greenland ice cores. *Journal of Geophysical Research: Atmospheres* 117 (D21), n/a-n/a.
- Dansgaard, W.; Johnsen, S. J., **1969**, A flow model and a time scale for the ice core from Camp Century, Greenland. *Journal of Glaciology* 8 (53), 215-223.
- Delmas, R. J., **1982**, Antarctic sulphate budget. *Nature* 299, 677-678.
- Ferris, D. G. *et al.*, **2011**, South Pole ice core record of explosive volcanic eruptions in the first and second millenia A.D. and evidence of a large eruption in the tropics around 535 A.D. *Journal of Geophysical Research* 116, D17308.

- Gao, C. *et al.*, **2006**, The 1452 or 1453 A.D. Kuwae eruption signal derived from multiple ice core records: Greatest volcanic sulfate event of the past 700 years. *Journal of Geophysical Research* 111 (D12).
- Graeter, K. A. *et al.*, **2018**, Ice Core Records of West Greenland Melt and Climate Forcing. *Geophysical Research Letters* 45 (7), 3164-3172.
- Hammer, C. U., **1977**, Past volcanism revealed by Greenland Ice Sheet impurities. *Nature* 270, 482-486.
- Herron, M., **1982**, Impurities sources of F⁻, Cl⁻, NO₃⁻, and SO₄²⁻ in Greenland and Antarctic precipitation. *J Geophys Res* 87, 3052-3060.
- Jauhiainen, T. *et al.*, **1999**, Simple procedure for ion chromatographic determination of anions and cations at trace levels in ice core samples. *Anal Chim Acta* 389, 21-29.
- Johnson, J. A. *et al.*, **2017**, Next generation of an intermediate depth drill. *Annals of Glaciology* 55 (68), 27-33.
- Kahle, E. C. *et al.*, **2021**, Reconstruction of Temperature, Accumulation Rate, and Layer Thinning From an Ice Core at South Pole, Using a Statistical Inverse Method. *Journal of Geophysical Research: Atmospheres* 126 (13).
- Kennedy, J. A., **2020**, Volcanic Impact on Stratospheric Chlorine Chemistry and Perchlorate Formation: Evidence from Ice Cores. South Dakota State University,
- Kiehl, J. T.; Brieglab, B. P., **1993**, The Relative Roles of Sulfate Aerosols and Greenhouse Gases in Climate Forcing. *Science* 260 (5106), 311-314.
- Kirchner, S.; Delmas, R. J., **1988**, A 1000 Year Glaciochemical Study at the South Pole. *Annals of Glaciology* 10, 80-84.
- Langway, C. C., **2008**, The history of early polar ice cores. *Cold Regions Science and Technology* 52 (2), 101-117.
- Legrand, M. In *Sulphur-Derived Species in Polar Ice: A Review*, Berlin, Heidelberg, Springer Berlin Heidelberg: Berlin, Heidelberg, 1995; pp 91-119.
- Legrand, M. *et al.*, **1984**, Ion chromatographic determination of common ions at ultratrace levels in Antarctic snow and ice. *Anal Chim Acta* 156, 181-192.
- Legrand, M.; Delmas, R. J., **1984**, The ionic balance of Antarctic snow: a 10 year detailed record. *Atmos. Environ.* 18, 1867-1874.
- Legrand, M.; Mayewski, P., **1997**, Glaciochemistry of polar ice cores: A review. *Reviews of Geophysics* 35 (3), 219-243.

- Lilien, D. A. *et al.*, **2018**, Holocene Ice-Flow Speedup in the Vicinity of the South Pole. *Geophysical Research Letters* 45 (13), 6557-6565.
- Manning, S. W. *et al.*, **2006**, Chronology for the Aegean Late Bronze Age 1700–1400 B.C. *Science* 312, 565-569.
- McAneney, J.; Baillie, M., **2019**, Absolute tree-ring dates for the Late Bronze Age eruptions of Aniakchak and Thera in light of a proposed revision of ice-core chronologies. *Antiquity* 93 (367), 99-112.
- Millero, F. J. *et al.*, **2008**, The composition of Standard Seawater and the definition of the Reference-Composition Salinity Scale. *Deep Sea Research Part I: Oceanographic Research Papers* 55 (1), 50-72.
- Mitchell, J. M., **1961**, Recent Secular Changes of Global Temperature. *Annals New York Academy of Sciences* 95, 235-250.
- Mosley-Thompson, E., **1996**; Holocene climate change recorded in an East Antarctica ice core. In *Climate Variations and Forcing Mechanisms of the last 2000 years*, Jones, P. D.; Bradley, R. S.; Jouzel, J., Eds. Springer-Verlag: New York, Vol. 41, pp 263-279.
- Mosley-Thompson, E.; Thompson, L. G., **1982**, Nine Centuries of Microparticle Deposition at the South Pole. *Quaternary Research* 17, 1-13.
- Osterberg, E. C. *et al.*, **2006**, Continuous Ice Core Melter System with Discrete Sampling for Major Ion, Trace Element, and Stable Isotope Analysis. *Environ Sci Technol* 40, 3355-3361.
- Palmer, A. S. *et al.*, **2002**, Antarctic Volcanic Flux Ratios from Law Dome Ice Cores. *Annals of Glaciology* 35.
- Petit, J. R. *et al.*, **1982**, A detailed study of snow accumulation and stable isotope content in Dome C (Antarctica). *Journal of Geophysical Research* 87 (C6).
- Robock, A., **2000**, Volcanic eruptions and climate. *Reviews of Geophysics* 38 (2), 191-219.
- Robock, A., **2003**; Volcanoes: Role in Climate. In *Encyclopedia of Atmospheric Sciences*, pp 2494-2500.
- Rodriguez-Gonzalez, A. *et al.*, **2009**, The Holocene volcanic history of Gran Canaria island: implications for volcanic hazards. *Journal of Quaternary Science* 24 (7), 697-709.
- Salzer, M. W.; Hughes, M. K., **2017**, Bristlecone pine tree rings and volcanic eruptions over the last 5000 yr. *Quaternary Research* 67 (1), 57-68.

- Sigl, M. *et al.*, **2016**, The WAIS Divide deep ice core WD2014 chronology – Part 2: Annual-layer counting (0–31 ka BP). *Climate of the Past* 12 (3), 769-786.
- Sofen, E. D. *et al.*, **2011**, The impact of anthropogenic emissions on atmospheric sulfate production pathways, oxidants, and ice core $\Delta^{17}\text{O}(\text{SO}_4^{2-})$. *Atmospheric Chemistry and Physics* 11 (7), 3565-3578.
- Sorge, E., **1932**, The Scientific Results of the Wegener Expeditions to Greenland. *The Geographical Journal* 81 (4), 333-344.
- Stebbins, A. K., A Special Report on the High Altitude Sampling Program. Agency, D. A. S. 1960
- Stothers, R. B., **1984**, The Great Tambora Eruption in 1815 and its Aftermath. *Science* 224 (4654), 1191-1198.
- The EPICA Dome C 2001-02 science and drilling teams, **2002**, Extending the ice core record beyond half a million years. *EOS* 83 (45), 509, 517.
- Traufetter, F. *et al.*, **2004**, Spatio-temporal variability in volcanic sulphate deposition over the past 2kyr in snow pits and firn cores from Amundsenisen, Antarctica. *Journal of Glaciology* 50 (168), 137-146.
- Vidal, C. M. *et al.*, **2016**, The 1257 Samalas eruption (Lombok, Indonesia): the single greatest stratospheric gas release of the Common Era. *Sci Rep* 6, 34868.
- Waugh, D. W. *et al.*, **2017**, What is the Polar Vortex and how does it influence weather. *American Meteorological Society*, 37-44.
- Winski, D. A. *et al.*, **2019a**, The SP19 chronology for the South Pole Ice Core – Part 1: volcanic matching and annual layer counting. *Climate of the Past* 15 (5), 1793-1808.
- Winski, D. A. *et al.*, **2019b**, Supplement of The SP19 chronology for the South Pole Ice Core – Part 1: volcanic matching and annual layer counting. *Climate of the Past* 15 (5), 1793-1808.
- Zach, How to Calculate Median Absolute Deviation in Excel. <https://www.statology.org/median-absolute-deviation-excel/> (accessed April 6, 2022).
- Zielinski, G. A. *et al.*, **1994**, Record of Volcanism Since 7000 B.C. from the GISP2 Greenland Ice Core and Implications for the Volcano-Climate System. *Science* 264 (5161), 948-952.